Silurian-Devonian magmatism, mineralization, regional exhumation and brittle strike-slip deformation along the Loch Shin Line, NW Scotland.

Holdsworth, R.E.[1], Dempsey, E.[1], Selby, D.[1], Darling, J.R.[2], Feely, M.[3], Costanzo, A.[3], Strachan, R.A.[2], Waters, P.[4], Finlay, A.J.[5], Porter, S.J.[6]

1=Department of Earth Sciences, Durham University, Durham, UK, DH1 3LE.
2= School of Earth and Environmental Sciences, University of Portsmouth, Portsmouth, PO1 3QL.
3= Earth and Ocean Sciences, School of Natural Sciences, Quadrangle Building, National University of Ireland, Galway, Ireland.
4=Eurasian Consolidated Minerals Pty Ltd, Level 1, 415 Riverside Road, Hawthorn East, Victoria 3123, Australia.
5=Origin Analytical, 1 Ravenscroft Court, Buttington Enterprise Park, Welshpool, SY21 8SL, UK.
6=Chemostrat, 1 Ravenscroft Court, Buttington Enterprise Park, Welshpool, SY21 8SL, UK.

ABSTRACT

The Loch Shin Line (LSL) is a geological-geophysical lineament associated with a zone of mantle-derived appinites, granites and strike-slip faulting that runs NW-SE across the Moine Nappe, N Scotland. U-Pb zircon and Re-Os molybdenite dating of the Loch Shin and Grudie plutons that lie immediately southwest of the NW-SE Loch Shin-Strath Fleet fault system yield ca. 427-430Ma ages that overlap within error. They also coincide with previously obtained U-Pb zircon ages for the Rogart pluton which lies along strike to the southeast. Field and microstructural observations confirm the similarity and contemporaneous nature of the plutons and associated sulphide mineralisation. Fluid inclusion analyses place further constraints on the P-T-X conditions during regional late Caledonian exhumation of the Moine Nappe. Synchronous to slightly younger brittle dextral strike slip faulting along the WNW-ESE Loch Shin-Strath Fleet Fault System was likely antithetic to sinistral movements along the nearby Great Glen Fault Zone. Our findings support the hypothesis that the LSL acted as a deep crustal channelway controlling the ascent and emplacement of Silurian magmas into the overlying Moine Nappe. We propose that this deep

structure corresponds to the southeastern continuation of the Precambrian-age Laxford Front shear zone in the buried Lewisian autochthon.

Supplementary material: [Field photographs, photomicrographs and fluid inclusion information] is available at www.geolsoc.org.uk/SUP0000

INTRODUCTION

Orogenic belts worldwide are characterized by interlinked systems of thrust, strike slip and extensional faults and, at deeper crustal levels, by shear zones that collectively accommodate crustal deformation in broad continental deformation zones during plate collision (i.e. 'block and flake tectonics'; Dewey *et al.* 1986). The location, geometry and persistence of faults and shear zones in such regions are known to be influenced by the reactivation of crustal-scale pre-existing structures (Sutton & Watson 1986; Holdsworth *et al.* 1997, 2001). These same structures are also known to act as channelways that control the upward migration and emplacement of hydrous mineralizing fluids and magmas (e.g. O'Driscoll 1986; Hutton 1988a; Jacques & Reavy 1994; Richards 2013). This coincidence of geological processes has greatly assisted in the analysis of orogenic deformation histories worldwide since dating of igneous intrusions and/or mineralization events using geochronology can also be used to constrain the absolute ages of associated deformation events in the adjacent wall rocks (e.g. Paterson & Tobisch 1988; Schofield & D'Lemos 1998; Rosenberg 2004).

Integrated structural and geochronological studies of deformed igneous intrusions have played a key role in constraining the timing of events within the Early Palaeozoic Caledonian orogeny in Scotland (Fig. 1a). Following Ordovician arc continent collision (the Grampian event), the final closure of Iapetus involved the oblique collisions of three palaeo-continents: Laurentia, Baltic and Avalonia during the mid- to late Silurian (e.g. Soper *et al.* 1992; Torsvik *et al.* 1996). In NW Scotland, regional deformation occurred due to the sinistral oblique Scandian collision of Baltica with Laurentia. Crustal thickening here was overlapped and followed by major sinistral displacements along orogen-parallel strike-slip faults such as the Great Glen Fault Zone (GGFZ; Fig 1a) heralding a transition from a regime of sinistral transpression to transtension (Dewey & Strachan 2003 and references therein). Igneous activity and associated mineralization related to slab breakoff was associated with this transition so that earlier granites were syn-tectonically emplaced along Scandian thrusts (e.g. Naver Thrust, see Holdsworth & Strachan 1988; Kinny et al 2003; Goodenough *et al.* 2011; Kocks *et al.* 2013), whilst later, volumetrically larger volumes of melt were emplaced along steeply-dipping strike-slip or normal faults (e.g. GGFZ; Hutton 1988b; Hutton & McErlean 1991; Jacques & Reavy, 1994; Stewart *et al.* 2001). In many cases the controlling faults or shear zones are exposed at the present-day surface, but others are more enigmatic features. As illustrated by Jacques & Reavy (1994) they are commonly inferred 'buried' structures based on geological, geophysical or geochemical alignments that define regional scale transverse lineaments that run generally at high angles to the orogenic strike. One of these NW-SE features, the Loch Shin Line (LSL) – first

defined by Watson (1984) – is associated with an anomalous zone of mantle-derived appinites, granites and brittle faulting in the Moine Nappe SE of the Moine Thrust on the N side of the Assynt Culmination (Fig. 1a, b). The LSL follows a strong NW-SE gravity gradient that defines the NE margin of a strong negative anomaly centred on the Grudie Granite (Figs 1b, see Leslie *et al.* 2010 and references therein). Watson (1984) suggested that the LSL corresponds to the presence of a Precambrian shear zone in the Lewisian autochthon underlying the Moine Nappe and that this shear zone has controlled the siting and ascent of magmas and associated mineralization during the Silurian. The dextral faulting that follows the trend of the LSL defines the Loch Shin, Strath Fleet and Dornoch Firth fault systems (Fig. 2a; Strachan & Holdsworth 1988) which are thought to be part of a regional fault set antithetic to the regional sinistral movements along the GGFZ (see Johnson & Frost 1977; Watson 1984). The Rogart igneous complex (Fig. 1a; Soper 1963), a large composite igneous intrusion of mantle derivation that lies on the NE margin of the LSL, is bounded to the SW by the Strath Fleet Fault. Kocks *et al.* (2013) have shown that emplacement of the central pluton – dated at 425±1.5 Ma using U-Pb (TIMS) zircon - was likely controlled by dextral motions along the LSL. These authors used this evidence to date the switch from sinistral transpression with thrusting to transtension with regional strike slip faulting at ca. 425 Ma.

The present paper re-examines this hypothesis in the region of Loch Shin where two plutons hosted in Moine and Lewisian country rocks are notably associated with molybdenite mineralization (Gallagher & Smith 1975): the Loch Shin and Grudie granites (Figs 1 & 2). Field observations and microstructural

100 studies are used to constrain the geometry, kinematics and relative ages of
101 deformation in the plutons and country rocks, whilst U-Pb zircon and Re-Os
102 molybdenite geochronology are used to date both pluton emplacement and the
103 spatially associated mineralization. Fluid inclusion studies are used to further
104 constrain the P-T-X conditions during deformation and igneous emplacement and
105 assess the relationships between regional structures and fluid flow.
106
107 ***GEOLOGICAL SETTING***
108 The Loch Shin area is underlain by variably deformed metsedimentary rocks of the
109 Morar Group, part of the Neoproterozoic Moine Supergroup in NW Scotland (Figs 1,
110 2; Holdsworth *et al.* 1994; Strachan *et al.* 2010). To the northwest, the Moine Nappe
111 is bounded by the underlying Moine Thrust and Moine Thrust Zone, whilst to the
112 north and east it is overlain by the Naver Thrust which carries the Loch Coire
113 Migmatite Complex (Fig. 1a; Kocks *et al.* 2013). Zircon U-Pb geochronology shows
114 that the migmatite complex formed during the Ordovician Grampian event ca 470-
115 460Ma (Kinny *et al.* 1999). This was followed by generally top-to-the-NW Scandian
116 ductile thrusting with early displacement along the Naver Thrust, then later thrusts
117 propagating progressively towards the Caledonian foreland ending with the
118 development of the Moine Thrust Zone (Barr *et al.* 1986; Johnson & Strachan 2006;
119 Alsop *et al.* 2010; Leslie *et al.* 2010). Zircon U-Pb dating of various syn-kinematic
120 igneous intrusions constrains thrust movements to ca. 435-425Ma (Kinny *et al.*
121 2003; Kocks *et al.* 2006; Goodenough *et al.* 2011). The broad arcuate swing of the
122 regional foliation and ductile thrusts within the Moine and Naver nappes (Fig. 1a,

123 2a) is attributed to the development of the Cassley structural culmination and
124 regional-scale flexuring in the rocks overlying the Assynt Culmination (Elliott &
125 Johnson 1980; Butler & Coward 1984; Leslie *et al.* 2010).

126 The Loch Shin and Grudie granites are hosted in Morar Group rocks locally
127 interleaved with antiformal isoclinal infolds of their underlying Lewisianoid
128 basement (Read *et al.* 1926; Gallagher & Smith 1975; Strachan & Holdsworth 1988;
129 Leslie *et al.* 2010). The Moine rocks are unmigmatized psammites interlayered with
130 subordinate semipelitic and pelitic horizons preserving rare sedimentary structures
131 such as cross-lamination and grading in areas of low tectonic strain. The
132 Lewisianoid rocks are lithologically diverse and include hornblendic and
133 quartzofeldspathic gneisses, amphibolites and subordinate units of ultramafic
134 hornblendite, together with thin strips of metasedimentary schist and marble (e.g.
135 Airde of Shin, Fig. 2a; see Strachan & Holdsworth 1988 and references therein).
136 Individual Moine-Lewisianoid boundaries – where exposed - are marked either by
137 the development of local basement conglomerates or by the development of mica-
138 rich 'tectonic schists' (Peacock 1975; Strachan & Holdsworth 1988).

139 The dominant structures in the Moine and Lewisianoid rocks are tight to
140 isoclinal D2 folds that carry an axial planar S2 crenulation fabric of an earlier
141 bedding parallel schistosity (S1). The main foliation is therefore a composite
142 S0/S1/S2 fabric which carries an ESE- to SE-plunging mineral extension lineation L2
143 (Strachan & Holdsworth 1988). This lineation is interpreted to lie parallel to the
144 regional direction of top-to-the-NW tectonic transport during Scandian thrusting
145 (e.g. Barr *et al.* 1986; Strachan *et al.* 2010). Associated regional metamorphism

146 during D2 in the Loch Shin area was within the low to mid-amphibolite facies (Soper
147 & Brown 1971; Strachan & Holdsworth 1988).

148 The Moine and Lewisianoid rocks around Lairg and Loch Shin are cut by a
149 number of granitic bodies, which include (from largest to smallest): the Grudie,
150 Claonel and Loch Shin intrusions (Fig. 2; Gallagher & Smith 1975), together with
151 numerous small associated sheets and plugs of similar composition. These fall into
152 two distinct groups: early foliated granodiorites (e.g. Claonel), thought to be directly
153 equivalent to parts of the Rogart igneous complex, and supposedly later, generally
154 unfoliated intrusions of pink adamellite including the Grudie and Loch Shin bodies.
155 The trace of the LSL is also marked by a concentration of small plugs and pipe-like
156 bodies of intermediate to ultramafic appinites known as the Ach'uaine hybrids (Fig.
157 1b; Read *et al.* 1925; Watson 1984). These also occur as comagmatic enclaves within
158 the ca. 425Ma central granodiorite of the Rogart igneous complex (Fowler *et al.*
159 2001; Kocks *et al.* 2013). Appinites are widely associated with late Caledonian
160 plutons throughout the Scottish Highlands and point to a significant mantle
161 contribution to this magmatism (e.g. see Fowler & Henney 1996; Fowler *et al.* 2008).

162 Regional mapping, stream sediment sampling and analysis of shallow
163 borehole cores in the Loch Shin-Grudie area has shown that low grade molybdenite
164 mineralization is associated with pyrite in thin post-foliation quartz veins cutting
165 both country rock and granites; subordinate chalcopyrite, fluorite, galena, barite and
166 sphalerite also occur (Gallagher & Smith 1975). This mineralization is spatially
167 associated with the granites, but Gallagher & Smith (op cit) suggest that it may also

168 have been significantly influenced by regional structures in the surrounding wall
169 rocks.

170 Between Loch Shin and the Moray Firth to the east, the Moine and Lewisian
171 rocks are cut by at least three major, sub-vertical brittle faults: the Loch Shin, Strath
172 Fleet and Dornoch Firth fault zones (Fig. 1a; Read *et al.* 1925, 1926; Strachan &
173 Holdsworth 1988; Kocks *et al.* 2013). Exposure of these fault zones is generally very
174 poor with only the Strath Fleet Fault previously studied in any detail (Soper 1963).
175 A series of NW-SE-trending steeply dipping crush zones were recognized that
176 overprint Moine country rocks, the Rogart igneous complex and unconformably
177 overlying Devonian basal conglomerates (middle Old Red Sandstone). There is
178 evidence for multiple fault movements, with cataclastic fault rocks included as clasts
179 within overlying Devonian conglomerates and minor intrusions that cut brittle fault
180 rocks whilst also being overprinted by later faulting (Soper 1963). However, there is
181 little published evidence to support the dextral shear sense inferred by many
182 authors along these NW-SE faults (e.g. Johnson & Frost 1977; Watson 1984),
183 although apparent regional offsets of regional boundaries in the Moine Nappe are
184 consistent with right-lateral movements along the Strath Fleet and Dornoch Firth
185 Faults (Fig 1a; Soper 1963; Strachan & Holdsworth 1988). A presumably late
186 (?Devonian) NE-side-down movement is also inferred for the Strath Fleet Fault
187 based on the preservation of Devonian conglomerates in an elongate NW-SE-
188 trending outlier that follows the Strath Fleet Valley (e.g. see Kocks *et al.* 2013).

189 There are no published structural studies of any of the igneous bodies that
190 occur close to Loch Shin due to the poor levels of exposure (<1%). The Grudie

pluton is inferred to cross-cut all ductile fabrics and geological boundaries in the Moine and Lewisian rocks based on the obviously discordant nature of the mapped boundaries and the absence of an internal foliation (Fig. 2b; Gallagher & Smith 1975).

The present study focusses on two key areas of exposure: a ca 1 km long sporadically continuous section through Moine rocks and part of the Loch Shin Granite on the southwest shore of Loch Shin; and isolated exposures of Grudie Granite exposed in road cuts related to the Meall a' Gruididh wind farm development (Fig. 2b).

LOCH SHIN GRANITE

Good quality water-washed exposures of Moine country rocks, the Loch Shin Granite and associated mineral veins occur along the SW shore of Loch Shin between NC 5650 0590 and NC 5625 0668 (Fig. 2b; see also Appendix A, Supplementary Material). Isolated poor quality exposures also occur in inland areas and stream sections, notably along the Allt a' Chlaonaidh (see Gallagher & Smith 1975, fig. 3).

Moine country rocks are exposed south of the Loch Shin granite between NC 5650 0590 and NC 0623 5638 and, north of the granite, between NC 5625 0668 and NC 5587 0766. They are mostly fine to medium grained grey mica psammites with a flaggy foliation and mm-scale compositional banding. Isolated layers of grey-brown weathering semipelite-pelite are sparsely developed in layers up to 20 cm thick. In thin section, the psammites comprise quartz, plagioclase, K feldspar, green biotite

and accessory phases (mineralization, garnet, epidote). Quartz and feldspar uniformly display sub-equant polygonal to cuspate-lobate textures typical of amphibolite facies conditions (e.g. see Holdsworth & Grant 1990), with the main banding parallel fabric (S0/S1/S2) being defined primarily by aligned biotite grains. The foliation and associated mineral lineations are locally variable in orientation – possibly due to the local effects of late brittle folding and faulting (see below) - but the majority strike NE-SW with moderate SE dips (Figs 2b, 3a). The associated fine mineral lineations, interpreted here as L2, plunge mainly ESE (Fig. 3a) typical of this part of the Moine Nappe in Sutherland (e.g. Strachan & Holdsworth 1988).

The ductile foliation in the Moine rocks is cross cut at low angles by generally NE-SW trending, moderately SE dipping pink granite and granite pegmatite sheets up to 1 m thick (e.g. Fig. 4b). These are unfoliated and are compositionally very similar to the Loch Shin granite.

The contacts of the Loch Shin granite are not exposed but are inferred to trend NE-SW and dip to the SE based on the orientation of the exposed granite-pegmatite veins (Figs 2b, 3b). The pink granite is typically fine to medium grained and is unfoliated, lacking both magmatic and solid-state ductile fabrics. In thin section it typically comprises weakly sericitised plagioclase, perthitic K-feldspar (occasionally as phenocrysts), quartz, biotite (often altered to secondary chlorite) and iron oxide (?magnetite). The granite is homogneous in terms of both composition and grain size and no internal contacts were seen. No magmatic-state fabric is present, nor is there any evidence of crystal plasticity other than low-temperature features spatially associated with fractures.

237 The granite is cut by irregular sets of quartz-pyrite-chalcopyrite veins with
238 rare molybdenite. These veins have no dominant orientation. However, at NC 5630
239 0660, a large sub-vertical SSE-NNW trending quartz-pyrite-sphalerite-chalcopyrite-
240 galena vein up to 1 m thick can be traced for over 10 metres along strike. All veins
241 lack ductile deformation fabrics, but are cross-cut by brittle faults and low
242 temperature cataclasis (e.g. Fig. 4a). Rice & Cope (1973) and Gallagher & Smith
243 (1975) give further details of veins and mineralization found in the surrounding
244 country rocks and report the additional presence of minor covellite, barytes and
245 fluorspar. Rare, late veins of zeolite <1 mm thick were observed cross-cutting fault-
246 related breccias in Moine host rocks (e.g. NC 5625 0668).
247 Widespread brittle deformation cuts Moine country rocks, the Loch Shin
248 Granite and associated granite-pegmatite veins alike (Figs 4a-f). The Loch Shin
249 Granite is cut by steeply-dipping, several metre long planar dextral faults trending
250 WNW-ESE with shallowly plunging slickenlines (Figs 3c, 4c). The total offsets are
251 unknown. Dextral faults are everywhere associated with shorter length, steeply-
252 dipping N-S to NE-SW sinistral faults with cm-scale offsets (Figs 3c, 4a) that either
253 abut against, or are cross-cut by dextral faults (Fig. 4d) suggesting that they are
254 contemporaneous. Irregularly oriented, mainly shallowly-dipping reverse faults
255 with prominent NNW- to SSE-plunging grooves & slickenlines are locally present in
256 the granite (e.g. around NC 5635 0630; Figs 3d, 4e). The fault planes are curviplanar
257 & lineated, with a series of ramp-flat configurations. Offsets are mostly small (mm-
258 cm scale). Once again these faults show mutually cross-cutting relationships with
259 the steeply dipping strike slip faults suggesting that they are broadly

contemporaneous. A stress inversion analysis of all fault slickenline data suggests a normal faulting to transtensional stress regime with a component of N-S shortening and E-W extension, consistent with regional-scale dextral shear along the Loch Shin Fault (Fig 3f).

In addition to brittle faults, both Moine rocks and granite are locally cut by metre-scale zones of brecciation and cataclasis, some of which appear to be associated with specific faults whilst others are diffuse and irregular. The banded Moine rocks locally preserve brittle-ductile box folds with generally moderate to steep easterly plunges (e.g. Figs 3e, 4f). These structures refold the ductile foliation (S2) and lineation (L2). The age of these folds relative to granite emplacement is uncertain, but one example appears to detach along a NE-SW sinistral fault suggesting that the folds are also post-granite features related to the regional brittle deformation. Such folds have not been observed within the granite, but this may reflect the lack of a pre-existing mechanical layering in these rocks.

In thin section, the effects of brittle deformation and cataclasis are widespread in all samples from the Loch Shin shore section (e.g. Figs 5a-f). Irregular networks of small-offset shear and hybrid fractures host variable amounts of mineralization and secondary alteration features including sericite and other clay minerals, quartz, chlorite, hematite, pyrite, chalcopyrite, limonite, fluorite and zeolite (e.g. Figs 5c, e, f). This suggests that the fractures have hosted significant volumes of fluid, an assertion supported by the widespread preservation of multiple sets of healed microfractures (Tuttle lamellae) in quartz in a wide range of orientations (Figs 5d, e). The presence of both pyrite and chalcopyrite in these

fracture fills suggest that at least some of the widely observed base metal mineralization was synchronous with brittle deformation. In several cases, sericite-filled fractures cutting feldspars are seen to pass laterally into well-defined Tuttle lamellae in adjacent quartz grains (Fig. 5e). Isolated veins of zeolite <1 mm thick cross cut all other brittle structures (Fig. 5f) and appear to represent the final phase of mineralization.

GRUDIE GRANITE

The Grudie Granite is poorly exposed and none of its contacts have been observed. In surface exposures, the granite is unfoliated, medium to fine grained, with sparse large phenocrysts of perthitic K-feldspar up to 1 cm across and large rounded xenocrysts of polycrystalline quartz up to 1 cm across (see Appendix B, Supplementary Material). These are set in a matrix of lightly to moderately sericitized plagioclase and quartz, with sparse K-feldspar, biotite and iron oxide. Little internal variation in grain size or mineralogy has been observed and internal contacts were not found.

In the field, well-developed joints carry epidote, chlorite, zeolite, iron and manganese oxides with slickenlines locally developed in a variety of orientations, mainly dip-slip or oblique slip. In thin section, the effects of brittle deformation are limited with small fractures filled mainly with epidote, white mica, chlorite and limonite. The overall level of fracturing is less intense than in the Loch Shin Granite.

ZIRCON U-Pb ISOTOPE ANALYSIS

306 *Sample, mineral separation and analytical protocols*

307 A representative sample of Loch Shin granite from the SW west shore of Loch Shin
308 (DS1-11; Fig. 2b, NC 5635 0625) was selected for Zircon U-Pb LA-ICP-MS
309 geochronology. The analytical detail for the U-Pb analysis, including zircon
310 reference materials, is presented in Appendix C (see also Darling *et al.* 2012). In
311 brief, zircons were separated from sample DS1-11 using traditional methods and
312 mounted in epoxy resion. Prior to Laser ablation (LA)-ICP-MS U-Pb isotope analyses
313 the were imaged via cathodoluminescence. Laser ablation (LA)-ICP-MS U-Pb isotope
314 analyses were undertaken at the University of Portsmouth, using a New Wave 213
315 nm Nd:YAG laser coupled with an Agilent 7500cs quadrupole ICP-MS.

316

317 *Results*

318 The zircons separated from sample DS1-11 are generally small (<120 μm in length).
319 The majority of the zircons possess euhedral to sub-euhedral prismatic forms, with
320 oscillatory or banded zonation textures as revealed by CL imaging (Fig. 6).
321 Approximately 15 percent of grains are significantly different, and have variable
322 habit from equant to elongate with sub-euhedral to anhedral forms. The CL textures
323 of these grains are also variable, including sector zonation, broad banding and
324 oscillatory zonation with spongy overgrowths. A total of 19 zircon grains were
325 analysed by LA-ICP-MS, including a range of textural types (Table I). Three analyses
326 were rejected due to high levels of ^{204}Pb (common Pb), which was not corrected for
327 during data reduction.

The majority of the analyzed grains yield Silurian ages, although there is one concordant analysis with a $^{207}Pb/^{206}Pb$ age of 1284 ± 19 Ma and three slightly discordant analyses with $^{207}Pb/^{206}Pb$ ages ranging from 1725 to 1771 Ma (Table I, Fig 7a; all age uncertainties given to two standard deviations). These older grains are of the equant, anhedral group and have Th/U ratios (0.4-0.6) that are significantly lower than the Silurian grains (Th/U = 0.9 to 1.5). Ten of the prismatic, more euhedral grains with oscillatory zonation textures yield $^{206}Pb/^{238}U$ ages ranging from 416 to 436 Ma (Fig. 7b). In combination, these grains yield a concordia age of 427.3 ± 3.7 Ma. Two additional analyses yielded discordant U-Pb isotope data, and fall on a discordia line between the younger concordant population and ca. 1700 Ma. These are interpreted as mixed analyses, which is supported by the observation of variable isotopic ratios in the time resolved signals. The 427.3 ± 3.7 Ma concordia age of the younger group of prismatic zircons, with CL textures (oscillatory or fine-banded) and Th/U ratios (0.9-1.5) typical of igneous zircon, is taken as the best estimate of intrusion age of the Loch Shin Granite (Fig. 8).

RHENIUM-OSMIUM MOLYBDENITE GEOCHRONOLOGY

Samples

Four molybdenite samples were collected for rhenium-osmium (Re-Os) geochronology to constrain the timing of sulphide mineralization associated with the Loch Shin and Gruide granite intrusions. Although molybdenite mineralization was noted in several places within the Loch Shin intrusion by Gallagher & Smith (1975) only one *in-situ* quartz-molybdenite vein was observed in the field (AF33-10;

NC 5614 0650; Fig. 2b). The ~1 cm quartz vein hosts minor fine grained (~1 mm) rosettes and disseminated molybdenite grains. No appreciable alteration selvage is present, with the exception of minor silicification, and chloritization of magmatic biotite.

Three additional samples were selected from the area around the Grudie granite. Molybdenite±pyrite mineralization sufficient for geochronological analysis was only observed in the neighboring Moine rocks adjacent to the intrusion (Fig. 2b). The mineralization post-dates all ductile Moine fabrics. Molybdenite mineralization is associated with and without quartz veins and, similar to the Loch Shin granite, wallrock alteration is limited to silicification, and chloritization of biotite in the Moine rocks. Molybdenite within quartz veins is fine grained (0.5 to 1mm) and occurs as disseminations and parallel to the boundary between the quartz vein and wallrock (AF01-11; AF02-11). Molybdenite also occurs as coatings along fractures (AF36-10).

Mineral separation and analytical protocols

Molybdenite separation and Re-Os analytical protocols follow the methodology described by Selby and Creaser (2004), and Lawley and Selby (2012). These are summarized in Appendix D.

Results

The four molybdenite samples from the Loch Shin (n = 1) and Grudie granites (n = 3) possess between ~1.6 and 8 ppm Re and 7.5 and 36 ppb ^{187}Os. All four

molybdenite samples yield ages identical within uncertainty (Table II; Figure 8), indicating that mineralization associated with the Loch Shin and the Grudie granite intrusions occurred during the upper mid-Silurian (ca. 428 – 430Ma).

FLUID INCLUSION ANALYSIS

Analytical protocols

Three molybdenite-bearing quartz veins from the Loch Shin Granite and wall rocks of the Grudie granite were studied in the Geofluids Research Laboratory at the National University of Ireland Galway (see Appendix E for analytical details). A petrographic classification scheme for the quartz-hosted fluid inclusions was developed using transmitted polarised light microscopy (Table III; see also Appendix F, Supplementary Material).

Fluid Inclusion Petrography

Molybdenite-bearing quartz veins were investigated from the Loch Shin Granite (one sample: AF33-10) and from the Moine wall rocks of the Grudie Granite (two samples: AF35-10 and AF02-11). The fluid inclusion petrographic study adopted the concept of fluid inclusion assemblages (FIA) described by Goldstein (2003), an approach that places fluid inclusions into assemblages interpreted to represent contemporaneous fluid trapping. Fluid inclusions (FIs) in all samples display ellipsoidal to irregular morphologies. Inclusions are commonly ~10 μm in longest dimension and show low degrees of fill (F=0.7-0.95). The degree of fill [F=vol. liquid / (vol. liquid + vol. vapour)] was measured by estimating the proportions of liquid

and vapour at 25°C and comparing to published reference charts (Shepherd *et al.*, 1985). Four inclusion types (*Type 1, Type 2, Type 3* and *Type 4*) have been identified hosted in vein quartz and their petrological characteristics are presented in Table III. The classification scheme is based on phase relations in fluid inclusions at room temperature.

- *Type 1* are two-phase liquid-rich (L>V) aqueous inclusions. They are abundant in all three samples, occurring in trails and in clusters and they commonly display subrounded to irregular shapes. They range from 9 μm to 25 μm in length and their degree of fill is ~0.70 to 0.95.
- *Type 2* are monophase aqueous fluid inclusions (L only), and are present in all samples. They occur in trails alongside Type 1 FIs and range in longest dimension from 1 μm to 5 μm in length. These are interpreted as being metastable and indicate fluid trapping temperatures of < 50°C (Goldstein and Reynolds, 1994).
- *Type 3* are three-phase (L+L+V) aqueous-carbonic fluid inclusions. They are aligned within annealed fractures and occur as clusters or as isolated individuals. They exhibit subrounded to subangular morphologies that range between 4 and 17 μm in the longest dimension.
- *Type 4* are monophase (L) carbonic fluid inclusions. They are aligned within annealed fractures and also occur in clusters associated with Type 3 aqueous-carbonic inclusions. They range between 5 and 10 μm in longest dimension and possess rounded to sub-rounded morphologies. They are rare

and have been observed in samples AF33-10 (Loch Shin Granite) and AF02-11 (Grudie Granite).

Fluid Inclusion Microthermometry

In sample AF33-10 from the Loch Shin Granite, T_{FM} values for Type 1 range from -50.5° to -45.5°C. This temperature interval indicates the probable presence of NaCl and $CaCl_2$ (Shepherd *et al.*, 1985). T_{LM} values are from -13.5 to -1.1°C yielding salinities ranging from ~ 1.9 to 17.3 eq. wt. % NaCl (mean 9.7 eq. wt. % NaCl). Fluid inclusions homogenise to the liquid state between 119°-170°C (Table III, Fig. 9a).

T_{FM} values for Type 1 in sample AF02-11 from the Grudie Granite wall rocks range between -23° and -22.5°C corresponding to the eutectic point of the H_2O-NaCl±KCl system. T_{LM} values range from -3.60 to -0.70°C yielding salinities of ~3.7 to 6.9 eq. wt. % NaCl (mean 5.4 eq. wt. % NaCl). Homogenization to the liquid state occurs between 214° and 279°C. In sample AF35-10 T_{LM} values for Type 1 range from -4.3° to -2.2°C yielding salinities ranging from ~1.2 to 5.9 eq. wt. % NaCl (mean 4.4 eq. wt. % NaCl) Type 1 FIs homogenise to the liquid state between 151° and 244°C (Table III, Fig. 9a).

Type 3 aqueous-carbonic inclusions have been identified in all three samples but only microthermometry on Grudie Granite samples (AF02-11 and AF35-10) are reported here, because of the size (<3 microns) of these inclusions in the Loch Shin sample. CO_2 homogenisation (to the liquid state, and by meniscus fading at 31.10°C) occurs between 28° and 30.9°C yielding CO_2 densities that range between 0.47 and 0.65 gm/cc. CO_2 melting temperatures range from -56.6°C (the triple point for pure

442 CO_2) to -57.2°C, the latter indicates the presence of additional species (*e.g*. H_2S +H_2 –
443 see LRM results). Clathrate (CO_2 5.75 HO_2) melting takes place between +5.6° and
444 +9.9°C yielding aqueous phase salinities between ~0.2 and 8.1 eq. wt. % NaCl. Total
445 homogenization to the liquid state occurred between 214.2° and 279.5°C in sample
446 AF35-10, and between 262° and 308.2°C in sample AF02-11. Homogenization to the
447 vapour phase occurred in three inclusions in sample AF02-11 at ~332.7°C (Table III,
448 Fig. 9a).
449
450 *Laser Raman Microspectroscopy*
451 Laser Raman Microspectroscopy (LRM) was used to identify the phases present in
452 all fluid inclusion types observed in the three samples (Appendix G, Supplementary
453 Material) and revealed the presence of CO_2, N_2 and H_2S. LRM of Type 1 fluid
454 inclusions in all samples indicates the presence of CO_2. Type 3 FIs from the Grudie
455 granite wall rock samples have in addition to CO_2, trace amounts of H_2S and H_2. LRM
456 of Type 4 FIs from both granites indicates that they are composed of pure CO_2 with
457 trace amounts of H_2S.
458
459 *Interpretation*
460 The Mo-bearing veins from each of the granites contain a similar range of fluid
461 inclusion types, *i.e*. Types 1-4. Type 1 in the Grudie Granite wall rock veins display
462 similar fluid salinities that range between ~1 and 7 eq. wt. % NaCl. However, Type 1
463 from the Loch Shin Granite, display a significantly wider range of salinities *i.e*. ~2-18
464 eq. wt. % NaCl. This difference is coupled with T_H values for the Loch Shin sample

that are generally <180°C which contrasts markedly with the range recorded for Type 1 and 3 from the Grudie Granite wall rock veins (~180°-350°C). T_H histograms (Fig. 9a) for Type 1 and 3 fluid inclusions indicate a decrease in homogenization temperatures from Type 3 (~340°C) through Type 1 (~260°C) in the Grudie Granite wall rock veins to Type 1 (<180°C) fluid inclusions in the Loch Shin Granite vein. Bivariate plots of T_H and salinity show no obvious correlations, however, Type 1 inclusions from the Loch Shin Granite vein display an essentially isobaric variation in salinity (Fig. 9b). This low T isobaric trend displayed by the Loch Shin Type 1 inclusions is directly comparable to that displayed by high salinity fluids (Type 3) recorded in the Galway, Donegal, Newry and Leinster Granites in Ireland. Here, they are interpreted to represent basinal brines, sourced in overlying sedimentary basins, which circulated through the crystalline basement during a period of post-Caledonian crustal extension or transtension (see Conliffe *et al.* 2010 and references therein). It is arguable, therefore, that the Type 1 fluids recorded in the Loch Shin vein may post-date and be unrelated to Mo-mineralisation. Consequently P-T modelling using the fluid inclusion data is only performed for the Grudie Granite veins.

P-T Modelling

Grudie Granite wall rock veins: The molybdenite Re-Os chronometry shows that the mineralisation in both veins is contemporaneous and occurred ca. 428Ma. Accordingly, the timing of fluid trapping in AF02-11 and AF35-10 is considered to be broadly contemporaneous. Bulk fluid inclusion parameters were calculated using

488 the LRM results in combination with the microthermometric data, using the
489 computer programs CLATHRATES (Bakker, 1997) and FLUIDS (Bakker, 2003).

490 Isochores for the high and lower temperature Type 1 aqueous fluids and for
491 the Type 3 aqueous carbonic fluids in the two vein samples are presented in the P-T
492 diagram (Fig. 10). The field for Type 3 inclusions is defined by two isochores that
493 reflect their range of microthermometric data. Isochores for the lower and higher
494 temperature Type 1 aqueous fluids were constructed for salinities of ~4.5 and 5
495 eq.wt% NaCl matched with T_H values of ~176 and ~251°C, respectively
496 corresponding to their range of salinities and T_H values. The veins are spatially and
497 genetically related to the Grudie Granite which places constraints on the pressure
498 regime active during mineralisation. Ferguson and Al-Ameen (1985) calculated
499 pressures of 2.50±0.25kb for the aureole of the Omey Granite, Connemara which has
500 Mo mineralisation of a similar age and setting to the Grudie Granite (Feely *et al.*,
501 2007). These pressure constraints are used in Figure 10 to estimate trapping
502 temperatures for Type 3 fluids of ~340 to 410°C. Furthermore, Gallagher *et al.*,
503 (1992) used fluid inclusion microthermometry and stable isotope data to generate a
504 P-T model for Mo- mineralisation at the western end of the Galway Granite which
505 yielded pressures of 1.2 to 2.0kb and a temperature range of 360 to 450°C (see
506 Figure 10). A higher pressure and lower temperature regime prevailed during
507 Grudie Granite mineralisation indeed similar to that modelled for the Omey Granite
508 (Feely *et al.*, 2007). No evidence for fluid immiscibility was recorded in Type 1
509 inclusions and therefore they could have been trapped anywhere along their
510 respective isochores. Type 1 fluids are considered to be meteoric and trapped after ,

511 and at lower pressures than, the earlier magmatic aqueous carbonic Type 3
512 inclusions considered to be responsible for the Mo-mineralisation. The P-T history
513 of fluids in the Grudie Granite wall rock veins may have followed the path shown in
514 Figure 10 (black arrow).
515
516 **DISCUSSION**
517 *The relative and absolute ages of plutonism, mineralisation and deformation*
518 The U-Pb zircon and Re-Os molybdenite ages for the Loch Shin Granite and sulphide
519 mineralization associated with both plutons are all coincident and overlap almost
520 exactly within error (Fig. 8). These ages therefore confirm the geological
521 observations which suggest that the plutons and associated mineralisation are
522 contemporaneous and genetically related. The Loch Shin-Grudie granite ages
523 overlap within error with the U-Pb zircon (TIMS) age of 425 ± 1.5 Ma reported by
524 Kocks *et al.* (2013) for the central granodiorite of the Rogart pluton (Fig. 1a) which
525 was, according to these authors also emplaced contemporaneously with dextral
526 movements along the Strath Fleet Fault, the along strike southeastern continuation
527 of the Loch Shin Fault and the LSL (Fig. 1a).
528 The field and thin section observations suggest that the Loch Shin and Grudie
529 granites are petrologically similar – as suggested by previous authors (e.g. Gallagher
530 & Smith 1975). Both plutons post-date the ductile deformation fabrics in the
531 surrounding Moine and Lewisian rocks, including the main Scandian-age D2
532 structures. Both plutons are associated with a variety of ore mineralization,
533 including molybdenite and other base metal sulphides, and both are post-dated by

534 the effects of brittle deformation consistent with dextral transtensional movements
535 along the WNW-ESE-trending Loch Shin Fault. Unsurprisingly the intensity of this
536 brittle overprint is greater in the Loch Shin pluton, which lies closer to the main
537 fault trace.

538 The relative ages of the brittle faulting and mineralization are more complex.
539 Field and thin section observations of fracture-hosted sulphides (pyrite,
540 chalcopyrite) show that at least some of the base metal mineralization is
541 contemporaneous with the brittle deformation. The observations lend support to
542 the long-postulated proposal that the dextral movements along NW-SE faults such
543 as the Loch Shin, Strath Fleet and Dornoch Firth fault systems are contemporaneous
544 with, and antithetic to, regional sinistral movements along the GGFZ ca 425 Ma
545 (Johnson & Frost 1977; Watson 1984; Stewart *et al.* 2001). It also strengthens the
546 arguments of Dewey & Strachan (2003) and Kocks *et al.* (2013) that the switch from
547 regional sinistral transpression with thrusting to transtension with regional strike
548 slip faulting occurred at this time.

549 However, many brittle fractures also cross-cut mineral veins. Furthermore,
550 the Type 1 fluid inclusions seen as Tuttle lamellae in the Loch Shin granite are
551 clearly distinct from the fluid inclusion sets seen in the Grudie granite. Their
552 presence points to a somewhat later, near surface phase of fluid flow associated
553 with brittle dextral movements along the Loch Shin-Strath Fleet Fault system. Given
554 this specific association, it seems most likely that at least some dextral faulting and
555 fluid flow occurred over a protracted period into the Devonian (?Emsian, ca 410 Ma)

where it was associated with basin development and the very final stages of late Caledonian strike-slip faulting/transtension (cf. Dewey & Strachan 2003).

Pluton relationships at depth and the magnitude of dextral strike-slip faulting

The very poor levels of exposure in the Loch Shin-Lairg region make it difficult to ascertain how the various plutonic bodies in this area may be related in 3 dimensions. Gravity modelling by Hipkin & Hussain (1983) has ruled out the possibility that the large regional gravity low seemingly centred on the surface outcrop of the Grudie pluton (Fig. 1b) is due to the presence of a very large pluton at depth. More recent work by Leslie *et al.* (2010) suggests that the low occurs mainly due to the presence of a thick thrust culmination of Moine rocks (the Cassley Culmination, Fig. 2a) sitting structurally above and to the SE of the Assynt Culmination. Nevertheless, their gravity models suggest the presence of a shallowly buried pluton with horizontal dimensions of 7 x 11 km, with an average thickness of up to 3 km (see Leslie *et al.* 2010, fig. 10). Even allowing for significant errors in the calculations, these models indicate that the granites exposed in the Loch Shin-Lairg region (including the Grudie, Loch Shin, Claonel bodies) are likely to be underlain by a larger, possibly composite plutonic body located mainly to the SW of Loch Shin (Fig. 11a). It is tempting to suggest that this buried granite and the similarly composite Rogart body are part of a single pluton offset by dextral strike-slip faulting. However, this would require right lateral displacement of at least 10 km which seems at odds with other regional evidence. For example, the observed offsets of regional markers such as the nearby Loch Shin Lewisian inlier (Fig 2a)

579 suggest displacements of no more than a few hundred metres, as does the
580 observation that the Loch Shin Fault does not appear to continue very far to the NW
581 beyond the end of Loch Shin (Leslie *et al.* 2010). It seems more likely therefore that
582 the two plutons are separate, composite bodies located either side of the Loch Shin-
583 Strath Fleet fault system in a manner rather similar to other Caledonian plutons that
584 are associated with regional strike-slip fault zones in NW Scotland, most notably the
585 GGFZ (e.g. Hutton 1988b; Jacques & Reavy 1994; Stewart *et al.* 2001).
586
587 *Implications for the nature and significance of the Loch Shin Line*
588 The present study lends support to the suggestion of Watson (1984) that the NW-SE
589 trending Loch Shin Line (LSL) is associated with an anomalous zone of broadly
590 contemporaneous mantle-derived appinites, granites (Rogart, Grudie, Loch Shin and
591 many smaller satellite bodies) intruded ca. 425-428 Ma. These are postdated by
592 slightly younger (perhaps as young as ca 410 Ma) brittle dextral faulting in the
593 Moine Nappe SE of the Moine Thrust (Loch Shin-Strath Fleet and Dornoch Firth
594 faults, Fig. 1b). Watson (1984) suggested that the LSL corresponds to the location of
595 a Precambrian shear zone in the Lewisian autochthon underlying the Moine Nappe
596 which acted as a deep crustal channelway controlling the ascent of magmas and
597 mineralization during the later stages of the Caledonian orogeny (see also the leaky
598 lower crustal fault block model of Jacques & Reavy 1994). The most obvious
599 candidate structure seen in the Lewisian Complex west of the Moine Thrust Zone is
600 the steeply S-dipping Laxford Front, the major shear zone that separates the

601 Rhiconich and Assynt terranes; this lies almost parallel to and along strike from the
602 trace of the LSL (Figs 1, 11b).
603
604 *Constraints on regional exhumation rates at the end of the Caledonian orogeny*
605 The PT estimates derived from the fluid inclusion study reported here (Fig. 10) can
606 be compared with those for peak metamorphism in the central part of the foreland-
607 propagating Scandian thrust wedge in Sutherland in order to provide constraints on
608 the rate of regional exhumation. Integrated metamorphic and isotopic studies and
609 thermal modelling suggest that peak metamorphic conditions in the vicinity of the
610 Naver Thrust of ca. 650°C and 5.5 kbar (Friend *et al.* (2000) were attained at c. 440-
611 435 Ma (Johnson & Strachan 2006; Thigpen *et al.* 2013). In contrast, this study has
612 established temperature-pressure conditions at the time (ca. 425 Ma) of Grudie
613 Granite mineralisation of c. 375°C and 2.5 kb. The contrasting pressure estimates
614 suggest that around 10 km thickness of crust was removed in c. 10-15 myr, easily
615 achieved at an erosion rate of less than or equal to 1mm a^{-1}. Essentially the same
616 erosion rate was derived by Johnson & Strachan (2006) from consideration of
617 isotopic data and the likely (Emsian) age of the oldest Old Red Sandstone strata to
618 rest unconformably on the Moine rocks.
619
620 *The regional significance of Caledonian molybdenite mineralization*
621 Intrusion-related molydenite mineralization is documented throughout the Scottish
622 and Irish Caledonian-Appalachian Orogen (Figure 1a inset). The broad timing and
623 fluid characteristics of intrusion-related Mo-mineralisation in the Loch Shin and

624 Grudie Granite veins (ca. 428 Ma) is temporally similar to that of the Ballachulish
625 and Kilmelford igneous complexes, including the Lagalochan porphyry Cu-Mo
626 system (ca. 433-426 Ma; Appendix H; Conliffe *et al.*, 2010), pre-dates that of the
627 Etive Igneous Complex (ca. 415 Ma; Porter and Selby, 2010), Shap granite (ca. 405
628 Ma; Selby *et al.*, 2008) and the earliest granite related Mo-mineralisation in the Irish
629 sector of the Caledonian-Appalachian Orogen (ca. 423Ma, Feely *et al.*, 2010). Fluid
630 inclusion data for these systems indicate that Mo-mineralization is ultimately
631 associated with aqueous-carbonic fluids, which has also been shown to be common
632 among Cu+Mo mineralization associated with late Caledonian magmatism (Kay
633 1985; Gallagher *et al.* 1992; Feely *et al.* 2007; Selby *et al.* 2008; this study; Feely &
634 Selby, unpub data; see Appendix I, Supplementary Material).

635 Gold mineralisation in Dalradian metamorphic rocks at Curraghinalt,
636 Northern Ireland (Parnell *et al.* 2000; Rice *et al.*, 2012) and Tyndrum, Scotland
637 (Pattrick *et al.* 1988; Curtis *et al.* 1993) has also been linked to aqueous-carbonic
638 magmatic fluids that may have been derived from an underlying Caledonian
639 intrusive. Although CO_2 has only an indirect role on gold mineralization
640 (Lowenstern 2001), it may play a significant role in magmatic fluid exsolution and
641 evolution, and may lead to concentrations of Au, Cu and Mo into the vapour phase
642 (Heinrich *et al.* 1999; Ulrich *et al.* 2001). As such, intrusion-related Mo (+Cu)
643 mineralization may warrant attention during future mineral exploration,
644 particularly for porphyry Cu–Mo-Au mineralization and additionally for
645 structurally-controlled Au-mineralisation distal from the intrusion. In this regard
646 combined fluid inclusion data, U-Pb and Re-Os geochronometry have shown that

prolonged granite-related molybdenite mineralisation in the Connemara region was accompanied by aqueous-carbonic fluids in the Omey Granite at ca. 423 Ma and later in the Galway Granite at ca. 410Ma (Murvey), ca. 407Ma (Mace Head) and ca. 380Ma (Costelloe; Feely *et al.*, 2007, 2010). Moreover, the earliest granite related Mo-mineralisation of the Omey Granite was also initiated while major orogen parallel structures, *e.g*. Great Glen and Southern Upland Fault systems (Dewey and Strachan, 2003) were active.

CONCLUSIONS

Using detailed field observations, microstructural studies, U-Pb zircon and Re-Os molybdenite geochronology and fluid inclusion analyses, we have shown that a suite of mid-Silurian (ca. 425-430 Ma) granite plutons (Grudie, Loch Shin, Rogart and many smaller associated bodies) are contemporaneous with base metal sulphide mineralization, including molybdenite. Synchronous to slightly younger (ca. 427-410Ma) brittle dextral strike slip faulting along the WNW-ESE Loch Shin-Strath Fleet Fault System was antithetic to regional sinistral strike-slip movements along the NE-SW trending GGFZ (Fig. 11a). More generally, the associated plutonism, mineralization and strike-slip faulting confirms the transition from regional-scale transpression to transtension during the mid-Silurian to early Devonian in NW Scotland as postulated by Dewey & Strachan (2003).

Our findings also lend support to the existence of the NW-SE trending Loch Shin Line and to the hypothesis of Watson (1984) that it has acted as a deep crustal channelway controlling the ascent and emplacement of Silurian granitic and

appinitic magmas into the overlying Moine Nappe (Fig. 11b). It seems very likely that this deep structure corresponds to the southeastern continuation of the Precambrian-age Laxford Front shear zone in the buried Lewisian autochthon. This further illustrates how pre-existing crustal structures can be persistently reactivated even when buried beneath much younger thrust nappes and influence directly the migration and emplacement of hydrous mineralizing fluids and magmas (e.g. Jacques & Reavy 1994; Richards 2013).

Acknowledgements

C. Ottley is thanked for logistical help in the field. We appreciate careful and considered reviews by A. Leslie and Anonymous, together with the editorial comments of J. MacDonald.

References

Alsop, G.I., Cheer, D.C., Strachan, R.A., Krabbendam, M., Kinney, P.D., Holdsworth, R.E. & Leslie, A.G. 2010. Progressive fold and fabric evolution associated with regional strain gradients: A case study from across a Scandian ductile thrust nappe, Scottish Caledonides. In: Law, R.D., Butler, R.W.H., Holdsworth, R.E., Krabbendam, M. & Strachan, R.A.. (eds) *Continental Tectonics and Mountain Building: The Legacy of Peach and Horne,* Geological Society, London, Special Publication, **335**, 255-276. DOI: 10.1144/SP335.12

Bakker, R.J., 2003. Package FLUIDS 1. Computer programs for analysis of fluid inclusion data and for modelling bulk fluid properties. *Chemical Geology*, **194**, 3-23.

693 Barr, D., Holdsworth, R.E. & Roberts, A M. 1986. Caledonian ductile thrusting within a
694 Precambrian metamorphic complex: the Moine of N.W. Scotland. *Bulletin of the*
695 *Geological Society of America,* **97,** 754-64.
696 Butler, R.W.H. & Coward, M.P. 1984. Geological constraints, structural evolution and
697 the deep geology of the NW Scottish Caledonides. *Tectonics,* **3,** 347-365.
698 Conliffe, J., Selby, D., Porter, S.J. & Feely, M., 2010. Re-Os molybdenite dates from the
699 Ballachulish and Kilmelford Igneous complexes (Scottish Highlands): age contraints
700 for late Caledonian magmatism. *Journal of the Geological Society, London,* **167,** 297-
701 302.
702 Curtis, S.F., Pattrick, R.A.D., Jenkin, G.R.T., Fallick, A.E., Boyce, A.J. & Treagus, J.E., 1993.
703 Fluid inclusion and stable isotope study of fault related mineralization in Tyndrum
704 area, Scotland. *Transactions of the Institute of Mining and Metallurgy* (Section B:
705 Applied Earth Science), **102**, 39-47.
706 Darling, J.R., Storey, C.D. & Engi, M. 2012. Allanite U–Th–Pb geochronology by laser
707 ablation ICPMS. *Chemical Geology*, **292-293**, 103–115, doi:
708 10.1016/j.chemgeo.2011.11.012.
709 Dewey, J. F. & Strachan, R. A. 2003. Changing Silurian-Devonian relative plate motion
710 in the Caledonides: sinistral transpression to sinistral transtension. *Journal of*
711 *Geological Society (London*), **160**, 219–229.
712 Dewey, J.F., Hempton, M.R., Kidd, W.S.F., Saroglu, F. & Şengör, A.M.C. 1986. Shortening
713 of continental lithosphere: the neotectonics of Eastern Anatolia – a young collision
714 zone. *In*: Coward, M.P. & Ries, A.C. (eds) *Collision Tectonics*, Geological Society of
715 London, Special Publication, **19**, 3-36.

716 Elliott, D. & Johnson, M.R.W. 1980. Structural evolution in the northern part of the
717 Moine thrust belt, NW Scotland. *Transactions of the Royal Society of Edinburgh: Earth*
718 *Sciences,* **71,** 69-96.
719 Feely, M., Selby, D., Conliffe, J., & Judge, M., 2007. Re–Os geochronology and fluid
720 inclusion microthermometry of molybdenite mineralisation in the late-Caledonian
721 Omey granite, western Ireland. *Trans. Inst. Min. Metall. B, Appl. Earth Sci*., 2007,
722 **116B**, 143–149.
723 Feely, M., Selby, D., Hunt, J. & Conliffe, J. (2010). Long-lived granite-related
724 molybdenite mineralisation at Connemara, western Irish Caledonides. *Geological*
725 *Magazine.* **147**, 886-894
726 Ferguson, C.C., Al-Ameen, S.I., (1985) C.C. Muscovite breakdown and corundum
727 growth at anomalously low fH_2O: a study of contact metamorphism and convective
728 fluid movement around the Omey granite, Connemara, western Ireland,
729 *Mineralogical Magazine*, **49,** 505-515.
730 Fowler, M.B. & Henney, P.J. 1996. Mixed Caledonian appinite magmas: implications for
731 lamprophyric fractionation and high Ba-Sr granite genesis. *Contributions to*
732 *Mineralogy and Petrology*, **126**, 199-215.
733 Fowler, M.B., Henney, P.J., Darbyshire, D.P.F. & Greenwood, P.B. 2001. Petrogenesis of
734 high Ba—Sr granites: the Rogart pluton, Sutherland. *Journal of the Geological Society,*
735 *London,* **158,** 521-534.
736 Fowler, M.B., Kocks, H., Darbyshire, D.P.F. & Greenwood, P.B. 2008. Petrogenesis of
737 high Ba—Sr granitoids from the Northern Highland Terrane of the British
738 Caledonian Province. *Lithos*, **105**, 129-148.

739 Friend, C.R.L., Jones, K.A. & Burns, I.M. 2000. New high pressure event in the Moine
740 Supergroup, northern Scotland: implications for Taconic (early Caledonian) crustal
741 evolution. *Geology*, **28,** 543-546.
742 Gallagher, M.J. & Smith, R.T. 1975 *Molybdenite mineralisation in Precambrian rocks,*
743 *near Lairg, Scotland.* Institute of Geological Sciences, 86pp.
744 Gallagher, V., Feely, M., Hoegelsberger, H., Jenkin, G. R. T. & Fallick, A. E., 1992.
745 Geological, fluid inclusion and stable isotope studies of Mo mineralization, Galway
746 Granite, Ireland. *Mineralium Deposita,* **27,** 314– 325.
747 Goldstein, R.H. & Reynolds, T.J., 1994. Systematics of fluid inclusions in diagenetic
748 minerals. *SEPM Short Course*, **31**, 199pp.
749 Goldstein, R.H., 2003. Re-equilibrium of fluid inclusions. *Mineralogical Association of*
750 *Canada, Short Course Series*, 9–53.
751 Goodenough, K.M., Millar, I.L., Strachan, R.A., Krabbendam, M. & Evans, J.A. 2011.
752 Timing of regional deformation and development of the Moine Thrust Zone in the
753 Scottish Caledonides: constraints from the U-Pb geochronology of alkaline
754 intrusions. *Journal of the Geological Society, London,* **168**, 99-114.
755 Heinrich C. A., Gunther D., Audetat A., Ulrich T. & Frischknecht R., 1999. Metal
756 fractionation between magmatic brine and vapor, determined by microanalysis of
757 fluid inclusions. *Geology*, **27,** 755–758.
758 Hipkin, R.G. & Hussain, A., 1983. *Regional gravity anomalies: Northern Britain*,
759 Institute of Geological Sciences, Reports, 82/10.
760 Holdsworth, R.E. & Grant, C.J. 1990. Convergence - related 'dynamic spreading' in a
761 mid-crustal ductile thrust zone: a possible orogenic wedge model. *In:* Knipe, R.J. &

762 Rutter, E.H. (eds.) *Deformation Mechanisms, Rheology and Tectonics.* Special
763 Publication of the Geological Society, London, **54,** 491-500.
764 Holdsworth, R.E. & Strachan, R.A 1988. The structural age and possible origin of the
765 Vagastie Bridge granite and associated intrusions, Central Sutherland. *Geological*
766 *Magazine,* **125,** 613-20.
767 Holdsworth, R.E. Strachan, R.A. & Harris, A.L. 1994. The Moine Supergroup. *In:*
768 Gibbons, W. & Harris, A.L. (eds) *A Revised Correlation of Precambrian Rocks in the*
769 *British Isles*. Geological Society of London, Special Report, **22,** 23-32.
770 Holdsworth, R.E., Butler, C.A. & Roberts, A.M. 1997. The recognition of reactivation
771 during continental deformation. *Journal of the Geological Society, London,* **154,** 73-
772 78.
773 Holdsworth, R.E., Stewart, M., Imber, J. & Strachan, R.A. 2001. The structure and
774 rheological evolution of reactivated continental fault zones: a review and case study.
775 *In:* Miller, J.A., Holdsworth, R.E., Buick, I.S. & Hand, M. (eds) *Continental Reactivation*
776 and *Reworking.* Special Publication of the Geological Society, London, **184,** 115-137.
777 Hutton, D.H.W. 1988a. Granite emplacement mechanisms and tectonic controls:
778 inferences from deformation studies. *Transactions of the Royal Society of Edinburgh:*
779 *Earth Sciences*, **79,** 245-255.
780 Hutton, D.H.W. 1988b. Igneous emplacement in a shear zone termination: the biotite
781 granite at Strontian, Scotland. *Geological Society of America Bulletin,* **100,** 1392-
782 1399.
783 Hutton, D.H.W. & McErlean, M.A. 1991. Silurian and Early Devonian sinistral
784 deformation of the Ratagain Granite, Scotland: constraints on the age of Caledonian

movements on the Great Glen Fault System. *Journal of the Geological Society of London,* **148,** 1-4.

Jacques, J.M. & Reavy, R.J. 1994. Caledonian plutonism and major lineaments in the SW Scottish Highlands. *Journal of the Geological Society, London,* **151,** 955-969.

Johnson, M.R.W. & Frost, R.T.C. 1977. Fault and lineament pattern in the Southern Highlands of Scotland. *Geologie en Mijnbouw,* **56,** 287-294.

Johnson, M.R.W. & Strachan, R.A. 2006. A discussion of possible heat sources during nappe stacking: the origin of Barrovian metamorphism within the Caledonian thrust sheets of NW Scotland. *Journal of the Geological Society, London,* **163**, 579-582.

Kay, E.A. 1985. *Hydrothermal Mineralization and Alteration of the Lagalochan Au-Cu-Mo Prospect, W. Scotland.* Unpublished PhD thesis, University of London.

Kinny, P.D., Friend, C.R.L., Strachan, R.A., Watt, G.R. & Burns, I.M. 1999. U-Pb geochronology of regional migmatites in East Sutherland, Scotland: evidence for crustal melting during the Caledonian Orogeny. *Journal of the Geological Society, London*, **156**, 1143-1152.

Kinny, P.D., Strachan, R.A., Rogers, G.R., Friend, C.R.L. & Kocks, H. 2003. U—Pb geochronology of deformed meta-granites in central Sutherland, Scotland: evidence for widespread Silurian metamorphism and ductile deformation of the Moine Supergroup during the Caledonian orogeny. *Journal of the Geological Society, London*, **160**, 259-269.

Kocks, H., Strachan, R.A. & Evans, J.A. 2006. Heterogeneous reworking of Grampian metamorphic complexes during Scandian thrusting in the Scottish Caledonides: insights from the structural setting and U-Pb geochronology of the Strath Halladale

808 Granite. *Journal of the Geological Society, London*, **163**, 525-538.
809 Kocks, H., Strachan, R.A., Evans, J.A. & Fowler, M.B. 2013. Contrasting magma
810 emplacement mechanisms within the Rogart igneous complex, NW Scotland, record
811 the switch from regional contraction to strike-slip during the Caledonian orogeny.
812 *Geological Magazine*, **151**, 899-915.
813 Lawley, C.J.M., & Selby, D. 2012. Re-Os Geochronology of Quartz Enclosed Ultra-fine
814 Molybdenite: Implications for Ore Geochronology, *Economic Geology,* **107,** 1499-
815 1506.
816 Leslie, A.G., Krabbendam, M., Kimbell, G.S. & Strachan, R.A. 2010. Regional-scale lateral
817 variation and linkage in ductile thrust architecture: the Oykell Transverse Zone, and
818 mullions, in the Moine Nappe, NW Scotland. *In*: Law, R.D., Butler, R./W.H.,
819 Holdsworth, R.E., Krabbendam, M. & Strachan, R.A. (eds) *Continental Tectonics and*
820 *Mountain Building: The Legacy of Peach and Horne*. Geological Society, London,
821 Special Publications, **335**, 359-381.
822 Lowenstern, J.B., 2001, Carbon dioxide in magmas and implications for hydrothermal
823 systems: *Mineralium Deposita*, **36,** 490-450.
824 O'Driscoll, E.S.T. 1986. Observations of the lineament - ore relation. *Philosophical*
825 *Transactions of the Royal Society, London*, **A317**, 195-218.
826 Pernell, J., Earls, G., Wilkinson, J. J., Hutton, D. H. W., Boyce, A. J., Fallick, A. E., Ellam, R.
827 M., Gleeson, S. A., Moles, N. R., Carey, P. F., & Legg, I. 2000. Regional Fluid Flow and
828 Gold Mineralization in the Dalradian of the Sperrin Mountains, Northern Ireland:
829 *Economic Geology*, **95,** 1389-1416.

830 Paterson, S.R. & Tobisch, O.T. 1988. Using pluton ages to date regional deformations;
831 problems with commonly used criteria. *Geology*, **16**, 1108-1111.
832 Pattrick, R.A.D., Boyce, A. J. & MacIntyre, R.M. 1988. Gold-silver vein mineralization at
833 Tyndrum, Scotland. *Mineralogy and Petrology*, **38,** 61-76.
834 Peacock, J.D. 1975. Slide rocks in the Moine of the Loch Shin area, northern Scotland.
835 Bulletin of the Institute of Geological Sciences, 49, 23-30.
836 Porter, S.J., Selby, D. 2010. Rhenium-Osmium (Re-Os) molybdenite systematics and
837 geochronology of the Cruchan Granite skarn mineralization, Etive Complex:
838 implications for emplacement chronology. *Scottish Journal of Geology*, **46,** 17-21.
839 Read, H.H., Ross, G., Phemister, J. & Lee, G.W. 1925. *The geology of the country around*
840 *Golspie, Sutherlandshire*. Memoir of the Geological Survey, Scotland. HMSO.
841 Read, H. H., Phemister, J. & Ross, G. 1926. *The Geology of Strath Oykell and Lower Loch*
842 *Shin.* Memoir of the Geological Survey, Scotland, HMSO.
843 Rice, C.M. & Cope, M.J. 1973. *The ore mineralogy of some rocks from the Loch Shin area.*
844 Institute of Geological Sciences, Mineralogy Unit Report, **125,** 7pp.
845 Rice C. M., Mark D. F., Selby D., Hill N. J. 2012. Dating vein-hosted Au deposits in the
846 Caledonides of N. Britain. Mineral Deposit Studies Groups meeting abstracts.
847 *Transactions of the Institute of Mining and Metallurgy Section B: Applied Earth*
848 *Science,* **121,**199–200.
849 Richards, J.P. 2013 Giant ore deposits formed by optimal alignments and
850 combinations of geological processes. *Nature Geosciences*, 1-6, doi.
851 10.1038/NGEO1920.
852 Rosenberg, C.L. 2004. Shear zones and magma ascent: a model based on a review of

the Tertiary magmatism in the Alps. *Tectonics*, **23**, 1-21.

Schofield, D. & D'Lemos, R.S. 1998. Relationships between syn-tectonic granite fabrics and regional P-T-t-d paths: an example from the Gander-Avalon boundary of NE Newfoundland. *Journal of Structural Geology*, **20**, 459-471.

Selby, D., Conliffe, J., Crowley, Q., & Feely, M., 2007. Geochronology (Re–Os and U–Pb) and fluid inclusion studies of molybdenite mineralisation associated with the Shap, Skiddaw and Weardale granites, UK. *Applied Earth Science (IMM Transactions section B)*, **117,** 11-28.

Selby, D., & Creaser, R.A., 2004. Macroscale NTIMS and microscale LA-MC-ICP-MS Re-Os isotopic analysis of molybdenite: Testing spatial restrictions for reliable Re-Os age determinations, and implications for the decoupling of Re and Os within molybdenite. *Geochimica et Cosmochimica Acta,* **68,** 3897-3908.

Shepherd, T.J., Rankin, A.H. & Alderton, D.H.M., 1985. *A practical guide to fluid inclusion studies*. Glasgow and London, Blackie, Glasgow, 239pp.

Soper, N.J. 1963. The structure of the Rogart igneous complex, Sutherland. *Quarterly Journal of the Geological Society of London*, **119**, 445-478.

Soper, N.J. & Brown, P.E. 1971. Relationship between metamorphism and migmatisation in the northern part of the Moine nappe. *Scottish Journal of Geology*, **7,** 305-325.

Soper, N.J., Strachan, R.A., Holdsworth, R.E., Gayer, R.A. & Greiling, R.O. 1992. Sinistral transpression and the Silurian closure of Iapetus. *Journal of the Geological Society, London,* **149,** 871-880.

875 Stewart, M., Strachan, R.A., Martin, M.W. & Holdsworth, R.E. 2001. Constraints on early
876 sinistral displacements along the Great Glen Fault Zone, Scotland: structural setting,
877 U-Pb geochronology and emplacement of the syn-tectonic Clunes tonalite. *Journal of*
878 *the Geological Society, London,* **158,** 821-830.
879 Strachan, R.A. & Holdsworth, R.E. 1988. Basement - cover relationships and structure
880 within the Moine rocks of central and southeast Sutherland. *Journal of the Geological*
881 *Society, London,* **145,** 23-36.
882 Strachan, R.A., Holdsworth, R.E., Krabbendam, M. & Alsop, G.I. 2010. The Moine
883 Supergroup of NW Scotland: insights into the analysis of polyorogenic supracrustal
884 sequences. In: Law, R.D., Butler, R.W.H., Holdsworth, R.E., Krabbendam, M. &
885 Strachan, R.A. (eds) *Continental Tectonics and Mountain Building: The Legacy of*
886 *Peach and Horne,* Geological Society, London, Special Publication, **335,** 233-254.
887 DOI: 10.1144/SP335.11
888 Sutton, J. & Watson, J.V. 1986. Architecture of the continental lithosphere.
889 Philosophical Transactions of the Royal Society, London, **A317,** 5-12.
890 Thigpen, J.R., Law, R.D., Loehn, C.L., Strachan, R. A., Tracy, R.J., Lloyd, G.E., Roth, B.L. &
891 Brown, S.J. (2013), Thermal structure and tectonic evolution of the Scandian
892 orogenic wedge, Scottish Caledonides: integrating geothermometry, deformation
893 temperatures and conceptual kinematic-thermal models. *Journal of Metamorphic*
894 *Geology*, **31**, 813–842. doi: 10.1111/jmg.12046.
895 Torsvik, T.H., Smethurst, M.A., Meert, J.G.,Van der Voo, R., McKerrow, W.S., Brasier,
896 M.D., Sturt, B.A. & Walderhaug. H.J., 1996. Continental break-up and collision in the

897 Neoproterozoic and Palaeozoic:A tale of Baltica and Laurentia. *Earth Science*
898 *Reviews*, **40**, 229-258.
899 Ulrich, T., Gunther, D., & Heinrich, C.A. 2001. The evolution of a porphyry Cu-Au
900 deposit, based on LA-ICPMS analysis of fluid inclusions: Bajo de la Alumbrera,
901 Argentina. *Economic Geology*, **96**, 1743–1774.
902 Watson, J.V. 1984. The ending of the Caledonian Orogeny in Scotland. *Journal of the*
903 *Geological Society of London,* **141,** 193-214.
904

905 **Figure captions**

906 **Figure 1a)** Regional geology map of the northern Scottish Highlands. Inset map
907 shows the relative positions of Laurentia, Baltica, Avalonia and Gondwana following
908 the closure of the Iapetus Ocean (Caledonide-Appalachian belt in black).
909 Abbreviations as follows: AC = Assynt Culmination; DFF = Dornoch Firth Fault; GGFZ
910 = Great Glen Fault Zone; LCM = Loch Coire Migmatite complex; LSSFF = Loch Shin -
911 Strath Fleet Fault ; MF = Moray Firth; MT = Moine Thrust; NT = Naver Thrust; ORS =
912 Old Red Sandstone; R = Rogart igneous complex.
913 **b)** Gravity map of the Lairg-Loch Shin area, with locations of appinnitic intrusions
914 (Achnuie hybrids, yellow dots), Laxford front and surface trace of Loch Shin Line
915 shown (after Watson 1984 and Leslie *et al.* 2010).
916

917 **Figure 2a)** Overview geological map of the Loch Shin area after Strachan and
918 Holdsworth (1988) & Leslie *et al.* (2010). Box shows location of map shown in
919 Figure 2b. G= Grudie, C = Claonel, LS = Loch Shin granites. L = Lairg; LSF = Loch Shin

Fault; AS = Aird of Shin. **b)** Simplified version of geology in the Loch Shin – Grudie area (after Gallagher & Smith 1975). Geochronology sample locations are shown. GB = Grudie Burn; CCB = Cnoc na Cloich-bhuaile; MG = Meall a' Ghruididh; AC = Allt a' Chlaonaidh.

Figure 3) Equal area stereoplots of structural data collected from the Loch Shin shore section. **a)** Ductile foliation (Sn/S2; great circles) and L2 mineral lineations (dots). **b)** Granite veins (solid great circles) and quartz veins (dashed great circles) and lineation on quartz vein (dot). **c)** Steep faults (great circles) and slickenlines (dots). **d)** Shallow faults (great circles) and slickenlines (dots). **e)** Box fold hinges (dots) and axial surfaces (great circles). **f)** Stress inversion analysis and Mohr plot of combined fault slickenline data with weighting added to include fault sizes. LSF = inferred local orientation of Loch Shin Fault.

Figure 4) Brittle structures cutting the Loch Shin granite and its Moine country rocks. **a)** Plan view of NE-SW sinistral fault offsetting granite and quartz vein (NC 5635 0631). **b)** Plan view of NW-SE dextral fault offsetting granite pegmatite vein in Moine psammites (NC 5639 0613). **c)** Oblique sectional view of long NW-SE trending dextral fault scarp in Loch Shin granite; inset shows sub-horizontal orientation of slickenlines on fault surface consistent with strike-slip fault movement (NC 5631 0650). **d)** NE-SW sinistral fault offsetting and being offset by NNW-SSE dextral faults in Loch Shin granite (NC 5635 0631). **e)** Shallowly NW-dipping flats and shorter SE-dipping ramps ('r') in exposed small displacement, top-

to-the-NW faults; inset shows plan view of corrugated, lineated fault surface with NW-SE slickenlines (NC 5635 0632). **f)** Plan view of steeply plunging conjugate box folds detaching along sub-vertical NE-SW sinistral fault in Moine psammites (NC 5638 0621).

Figure 5) Thin sections of brittle structures and mineralization cutting the Loch Shin granite and its country rocks. **a)** Small offset (<0.5mm) domino style reverse (top-to-the-NW) shear fractures (arrowed) cutting Loch Shin granite viewed in ppl (NC 5635 0632). **b)** Typical zone of cataclasis cross cutting Loch Shin Granite viewed in crossed polars (NC 5635 0632). **c)** Irregular region of quartz iron oxide-ilmenite (black) -pyrite (black, Py) –fluorite (Fl) mineralization in Moine psammites immediately to the northwest of the Loch Shin granite viewed in ppl (NC 5625 0666). **d)** Multiple sets of fluid inclusions following healed microcracks/Tuttle lamellae in quartz from the Loch Shin granite viewed in ppl (NC 5635 0632). **e)** Microfactures lined with sericite where they cross-cut feldspar (Fsp) passing laterally into healed microcracks/Tuttle lamellae in quartz (Qtz), in granite pegmatite vein, viewed in crossed polars (NC 5639 0613). **f)** Late zeolite vein (Z) cutting brecciated Moine psammite viewed in cross-polars (NC 5625 0666).

Figure 6) Cathodoluminescence images and SHRIMP II analysis positions for representative grains from grains selected for geochronology from the Loch Shin Granite sample. Also shown are the grain numbers, and 207Pb/206Pb ages for each analysis pit (uncertainties are two standard deviations; percentage discordance

966 shown in brackets).

967

968 **Figure 7 a, b)** Zircon U-Pb concordia plots from the Loch Shin granite.

969

970 **Figure 8)** Plot of the U-Pb zircon and Re-Os molybdenite dates including 2 sigma
971 uncertainty with decay constant uncertainty for the Loch Shin and Gruide granites.
972 Also given is the weighted average for the Re-Os molybdenite dates for the Gruide
973 granite. For sample locations, see Figure 2.

974

975 **Figure 9) a)** Histogram of TH values and **b)** bivariate plot of TH vs. salinity for Type
976 1 and Type 3 inclusions in samples AF02-11 and AF35-10 from the Grudie granite
977 and for Type 1 in sample AF33-10 from the Loch Shin granite.

978

979 **Figure 10)** Pressure-temperature space showing isochores for Type 1 and Type 3
980 fluid inclusions. Shaded area represents the field for Type 3 fluids defined by two
981 isochores. Isochores for the lower and higher temperature Type 1 aqueous fluids
982 are also shown and the parameters used for their construction are shown on the
983 isochores. Proposed *P-T* path for cooling history of fluids in Grudie Granite is shown
984 by the arrow. *P-T* field for aqueous carbonic fluids associated with the Mo
985 mineralisation at the western end of the Galway Granite is shown for comparison
986 after Gallagher *et al.*, (1992).

987

988 **Figure 11) a)** 3-D summary of the spatial relationships between the Rogart, Loch

989 Shin, Lairg and Grudie plutons (red) and brittle strike slip faults (grey) in the Loch
990 Shin-Strath Fleet-Dornoch Firth area. **b)** Highly simplified conceptual model
991 showing how the buried Laxford front shear zone below the Moine nappe gives rise
992 to the Loch Shin Line of focussed Silurian magmas and overlapping Silurian-
993 Devonian dextral strike-slip faults.
994
995 **Tables**
996 **Table I)** U-Pb data for Loch Shin granite.
997
998 **Table II)** Re-Os data for molybdenite from the Loch Shin and Gruide granites.
999
1000 **Table III)** Classification of fluid inclusion types and fluid inclusion micro-
1001 thermometric data from the Loch Shin and Gruide granites**.**
1002
1003

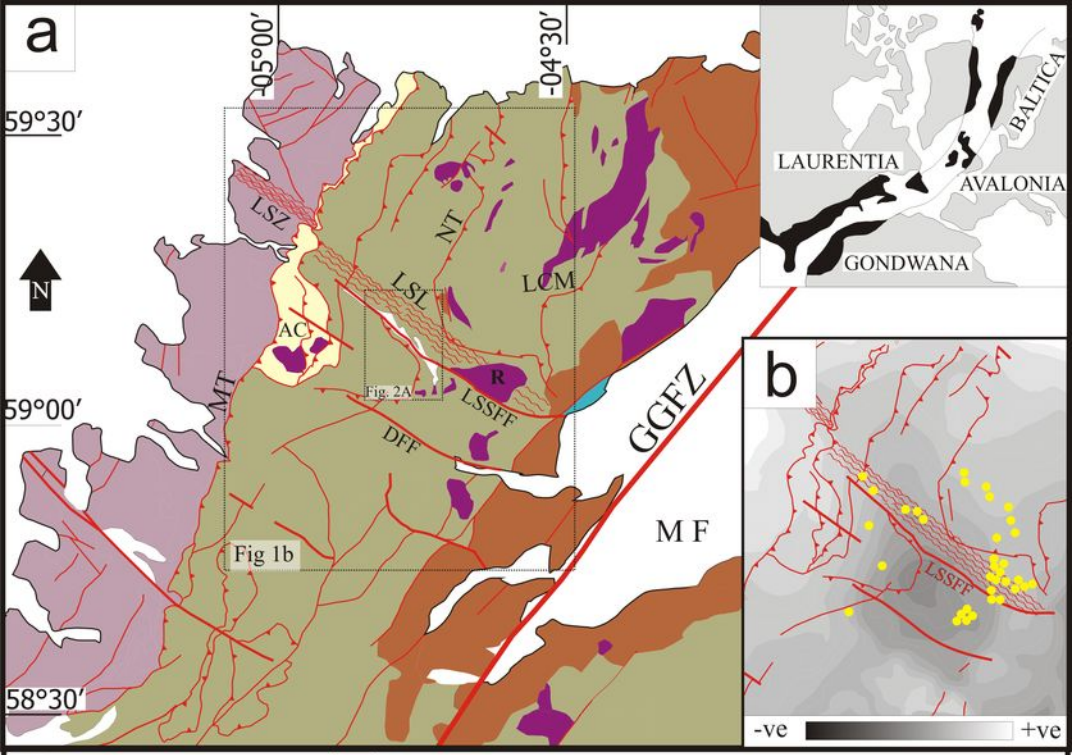
a
-05°00′
-04°30′
59°30′
59°00′
58°30′
N
LSZ
NT
LSL
LCM
AC
MT
Fig. 2A
R
LSSFF
DFF
GGFZ
M F
Fig 1b
LAURENTIA
BALTICA
AVALONIA
GONDWANA
b
LSSFF
-ve
+ve
Moine Supergroup
Caledonian Foreland
Moine Thrust Zone
Silurian -Devonian Granitoids
Devonian ORS
Jurassic Sediments
Fault
Thrust Fault
Basement Shear Zone / LSL
Appinites

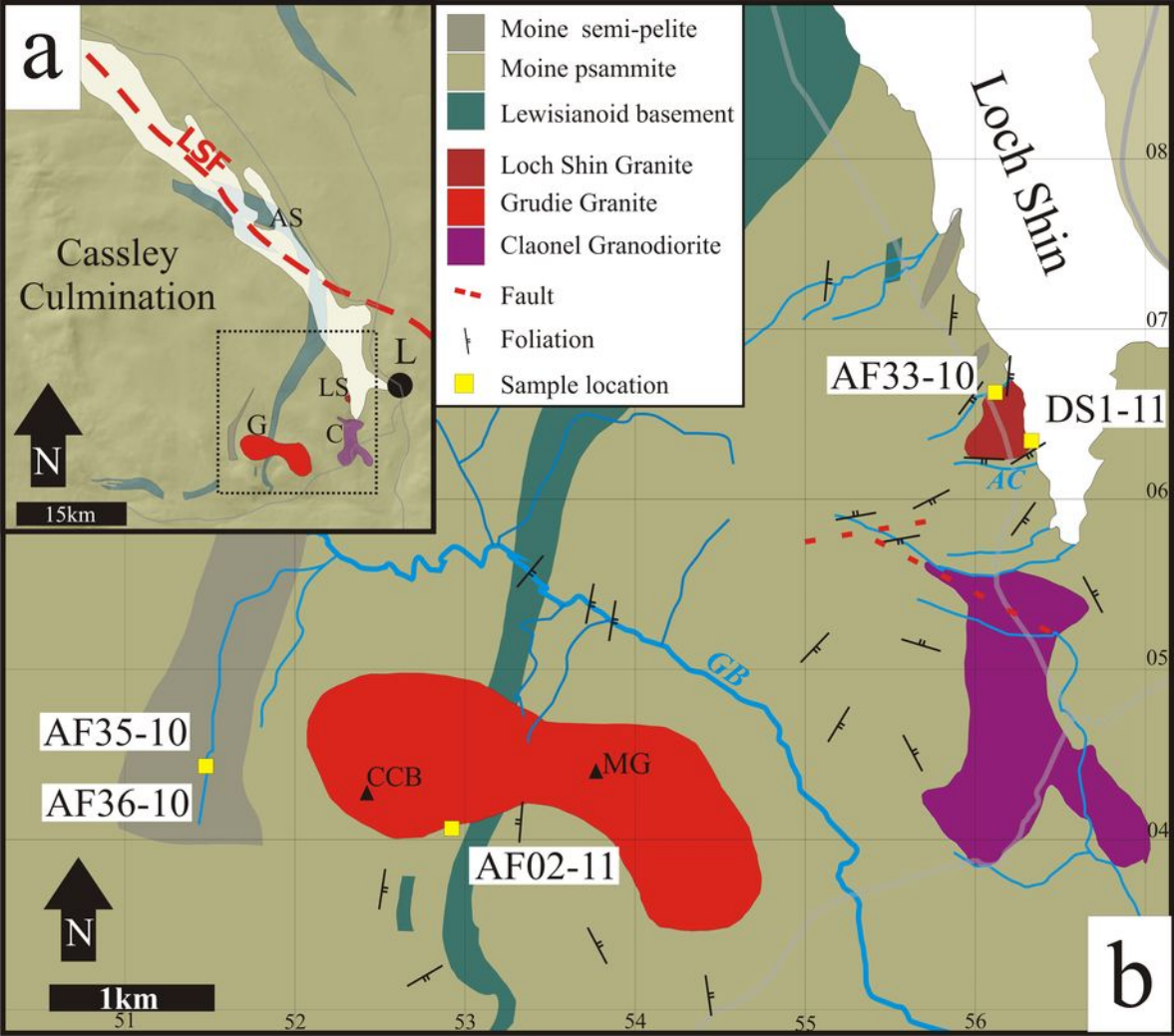
a
LSF
AS
Cassley
Culmination
L
LS
G
C
N
15km
Moine semi-pelite
Moine psammite
Lewisianoid basement
Loch Shin Granite
Grudie Granite
Claonel Granodiorite
Fault
Foliation
Sample location
Loch Shin
AF33-10
DS1-11
AC
GB
AF35-10
AF36-10
CCB
MG
AF02-11
N
1km
b
08
07
06
05
04
51
52
53
54
55
56

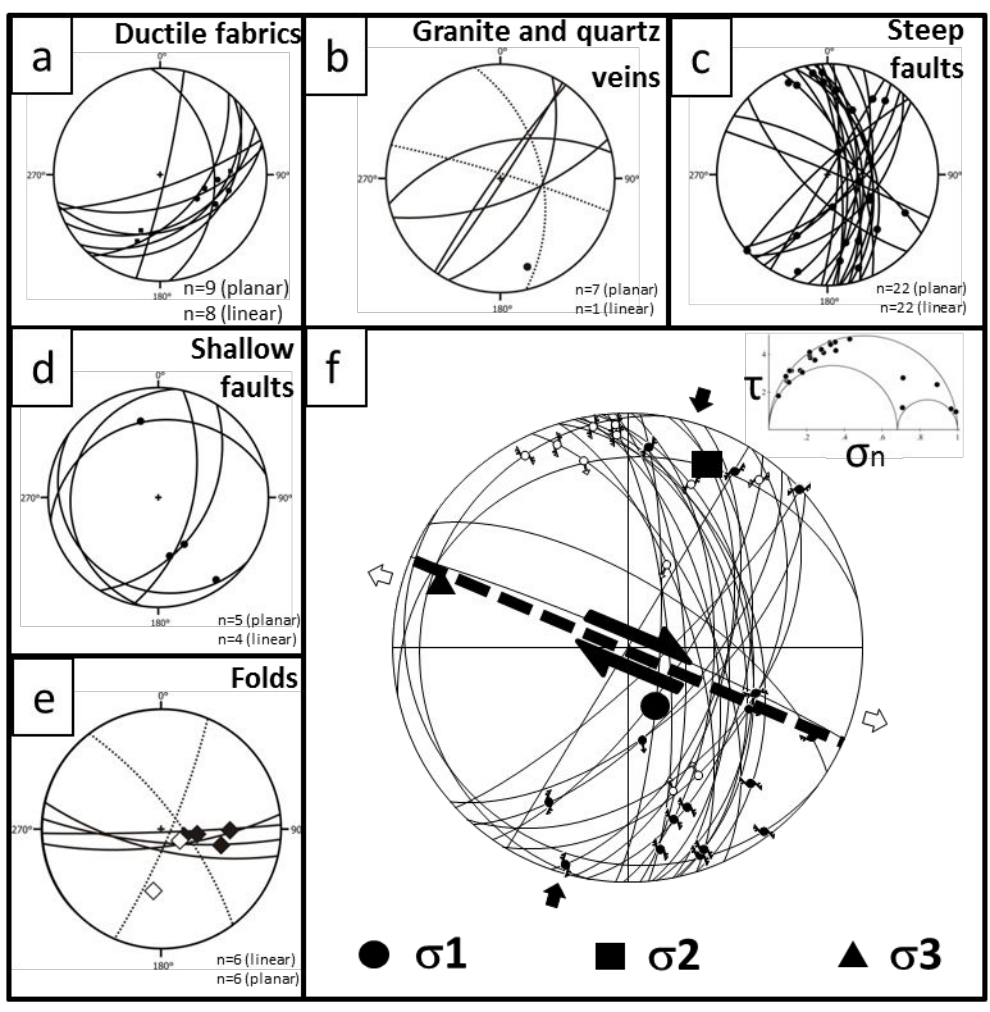
a
Ductile fabrics
n=9 (planar)
n=8 (linear)
b
Granite and quartz veins
n=7 (planar)
n=1 (linear)
c
Steep faults
n=22 (planar)
n=22 (linear)
d
Shallow faults
n=5 (planar)
n=4 (linear)
e
Folds
n=6 (linear)
n=6 (planar)
f
τ
σn
σ1
σ2
σ3

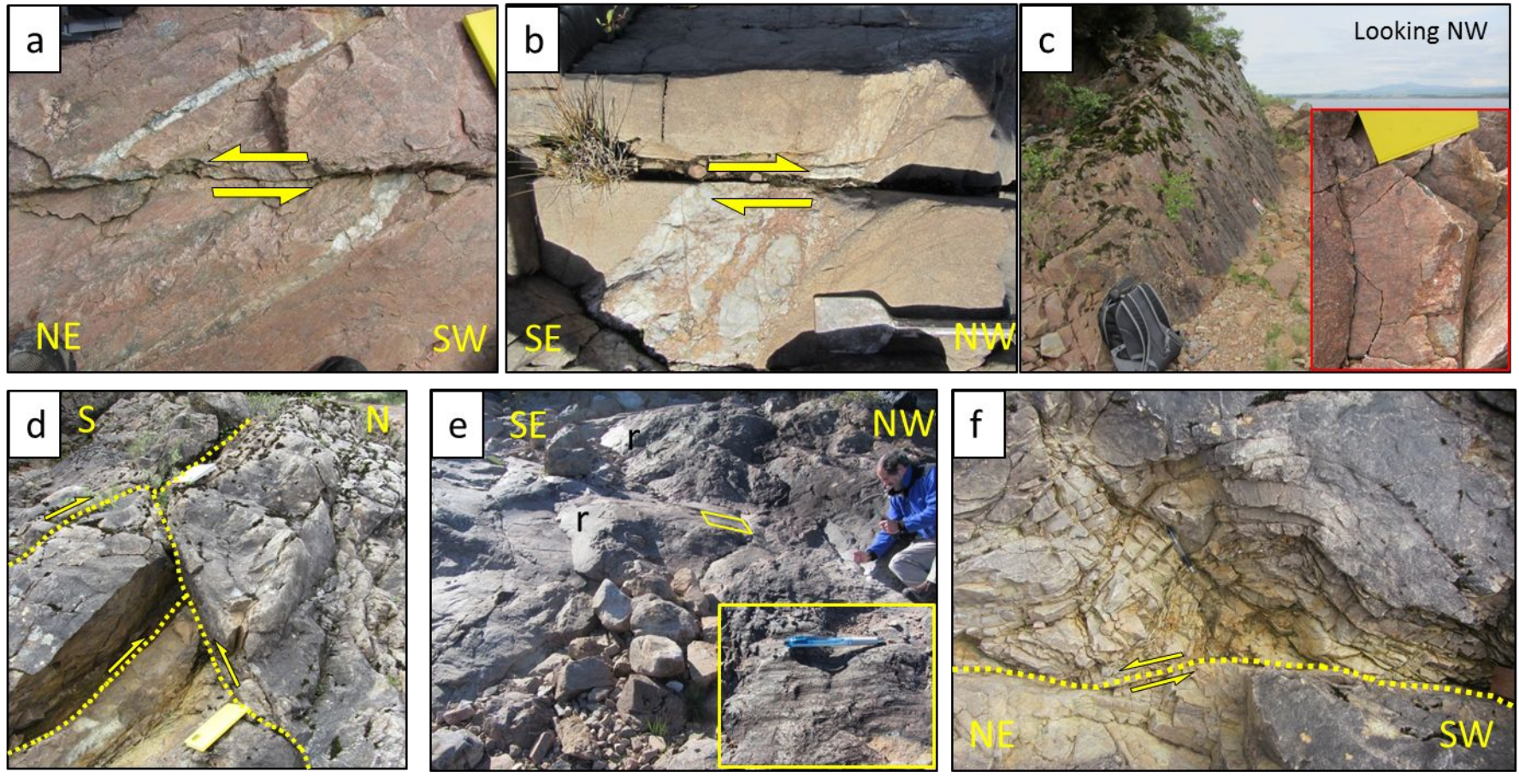
a
NE
SW
b
SE
NW
c
Looking NW
d
S
N
e
SE
NW
r
r
f
NE
SW

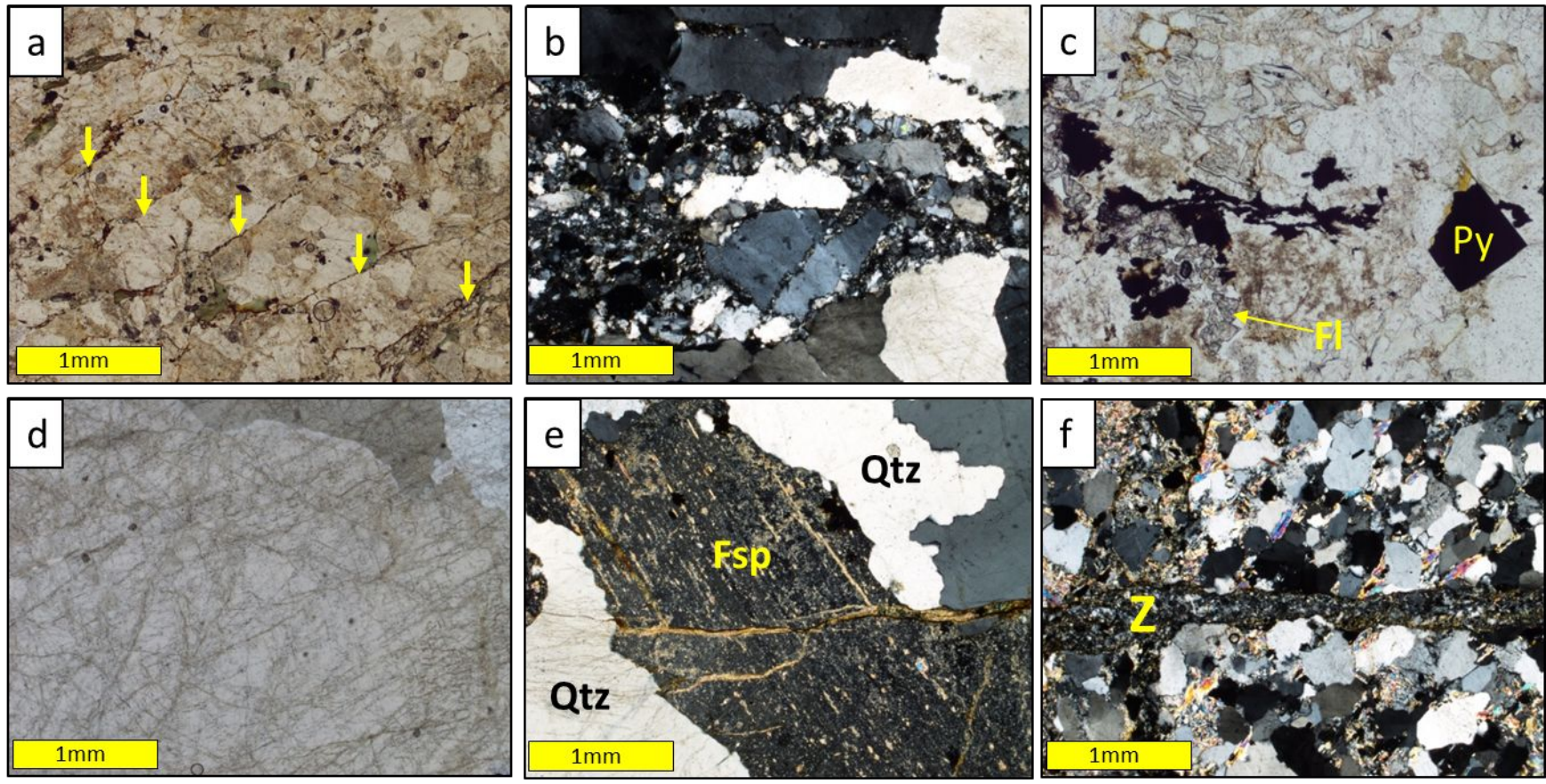
a
1mm
b
1mm
c
Py
Fl
1mm
d
1mm
e
Qtz
Fsp
Qtz
1mm
f
Z
1mm

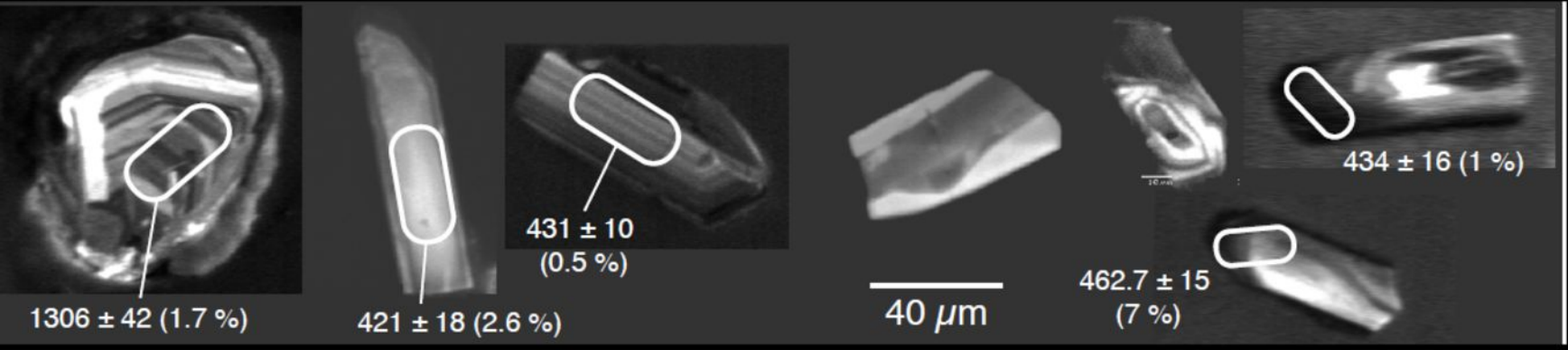
1306 ± 42 (1.7 %)
421 ± 18 (2.6 %)
431 ± 10
(0.5 %)
40 μm
462.7 ± 15
(7 %)
434 ± 16 (1 %)

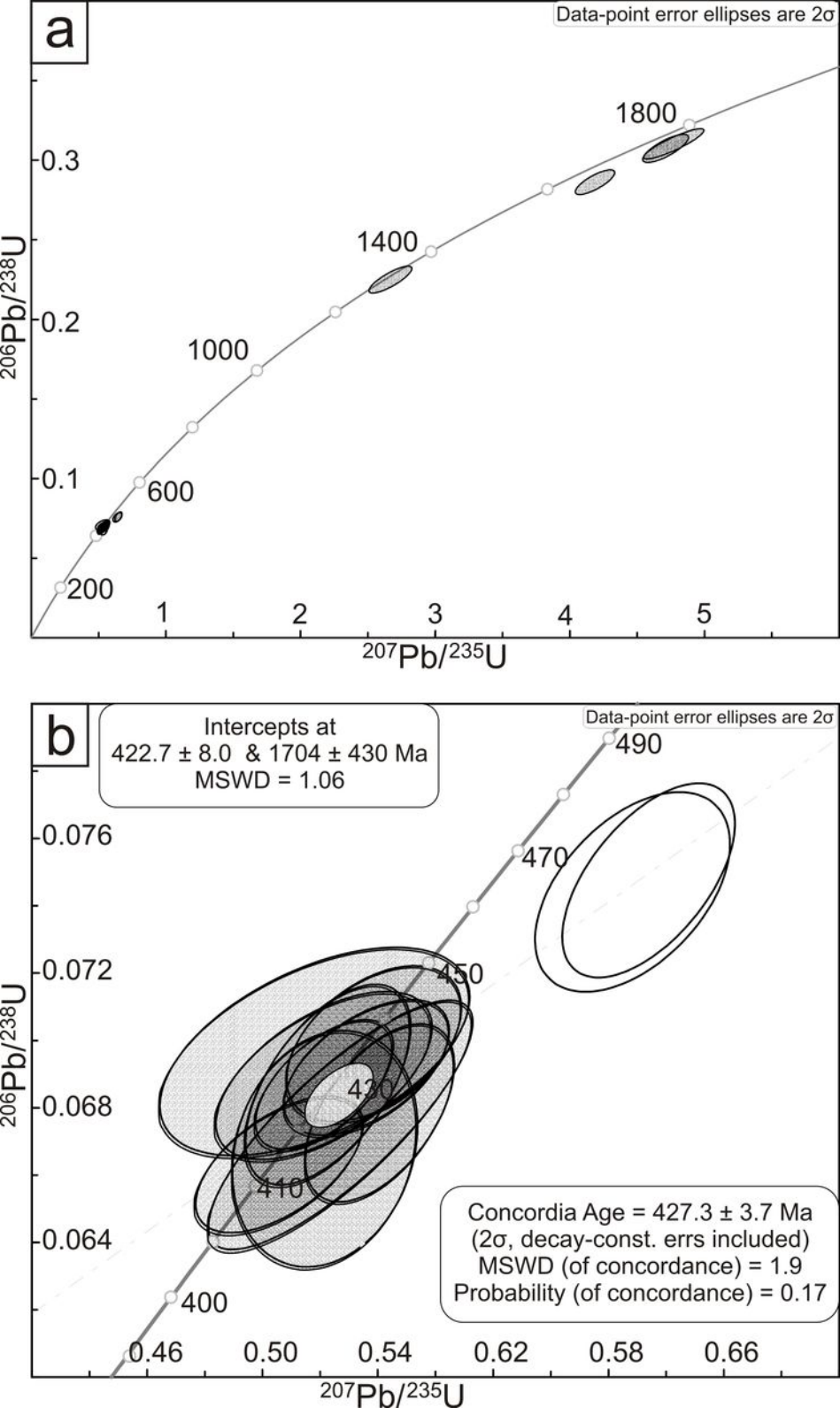
a
Data-point error ellipses are 2σ
1800
1400
1000
600
200
0.3
0.2
0.1
1
2
3
4
5
206Pb/238U
207Pb/235U
b
Intercepts at
422.7 ± 8.0 & 1704 ± 430 Ma
MSWD = 1.06
Data-point error ellipses are 2σ
490
470
450
430
410
400
0.076
0.072
0.068
0.064
0.46
0.50
0.54
0.62
0.58
0.66
Concordia Age = 427.3 ± 3.7 Ma
(2σ, decay-const. errs included)
MSWD (of concordance) = 1.9
Probability (of concordance) = 0.17
206Pb/238U
207Pb/235U

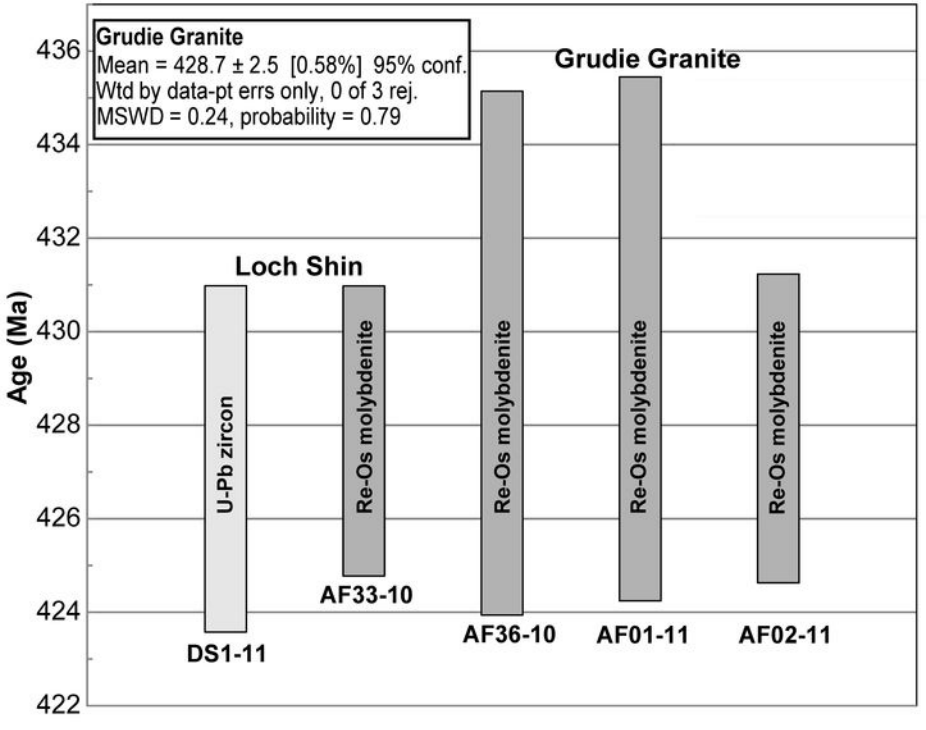
Grudie Granite
Mean = 428.7 ± 2.5 [0.58%] 95% conf.
Wtd by data-pt errs only, 0 of 3 rej.
MSWD = 0.24, probability = 0.79
Grudie Granite
Loch Shin
Age (Ma)
436
434
432
430
428
426
424
422
U-Pb zircon
Re-Os molybdenite
Re-Os molybdenite
Re-Os molybdenite
Re-Os molybdenite
DS1-11
AF33-10
AF36-10
AF01-11
AF02-11

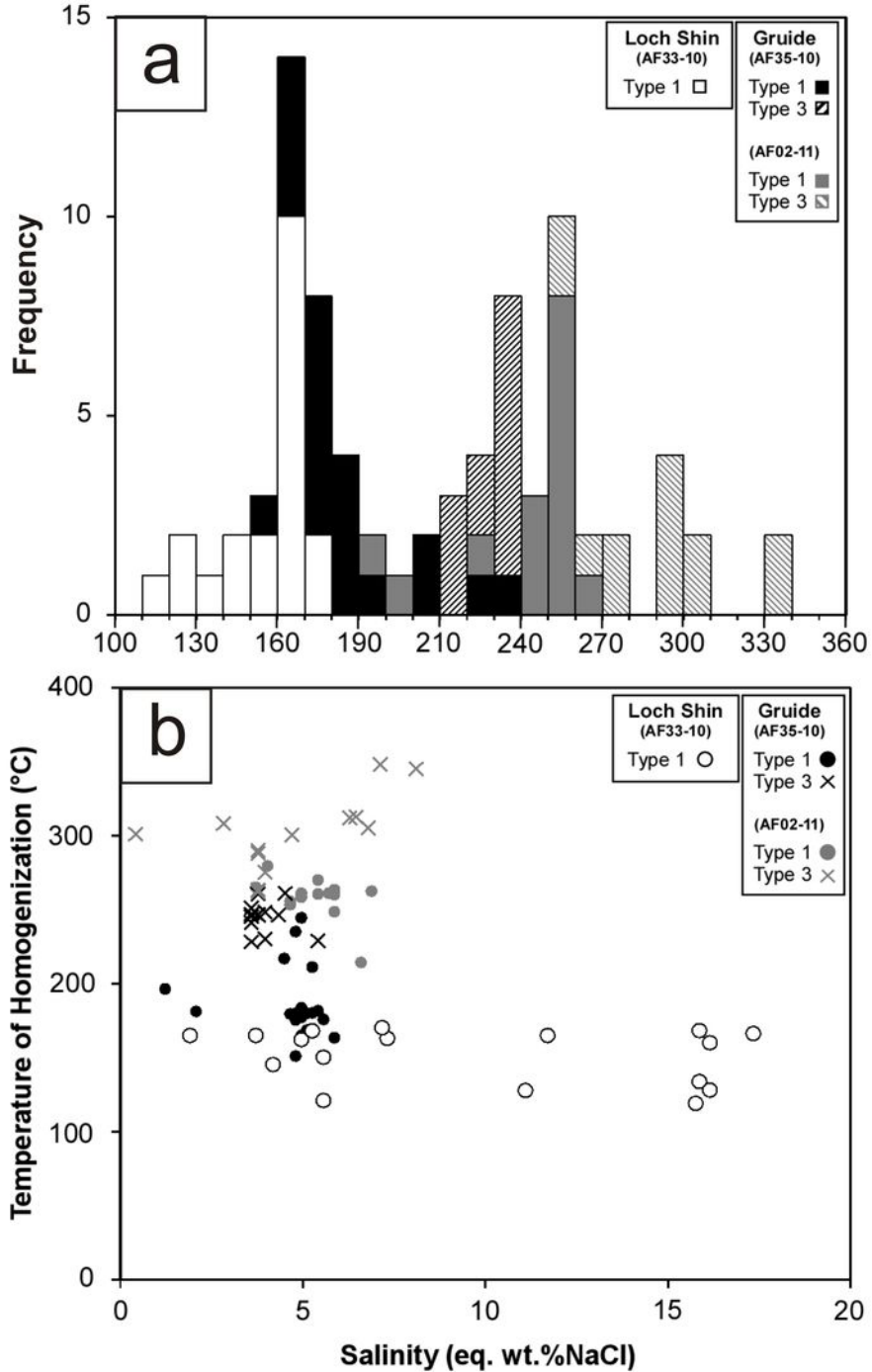
a
Loch Shin
(AF33-10)
Type 1
Gruide
(AF35-10)
Type 1
Type 3
(AF02-11)
Type 1
Type 3
Frequency
15
10
5
0
100
130
160
190
210
240
270
300
330
360
b
Loch Shin
(AF33-10)
Type 1
Gruide
(AF35-10)
Type 1
Type 3
(AF02-11)
Type 1
Type 3
Temperature of Homogenization (°C)
400
300
200
100
0
0
5
10
15
20
Salinity (eq. wt.%NaCl)

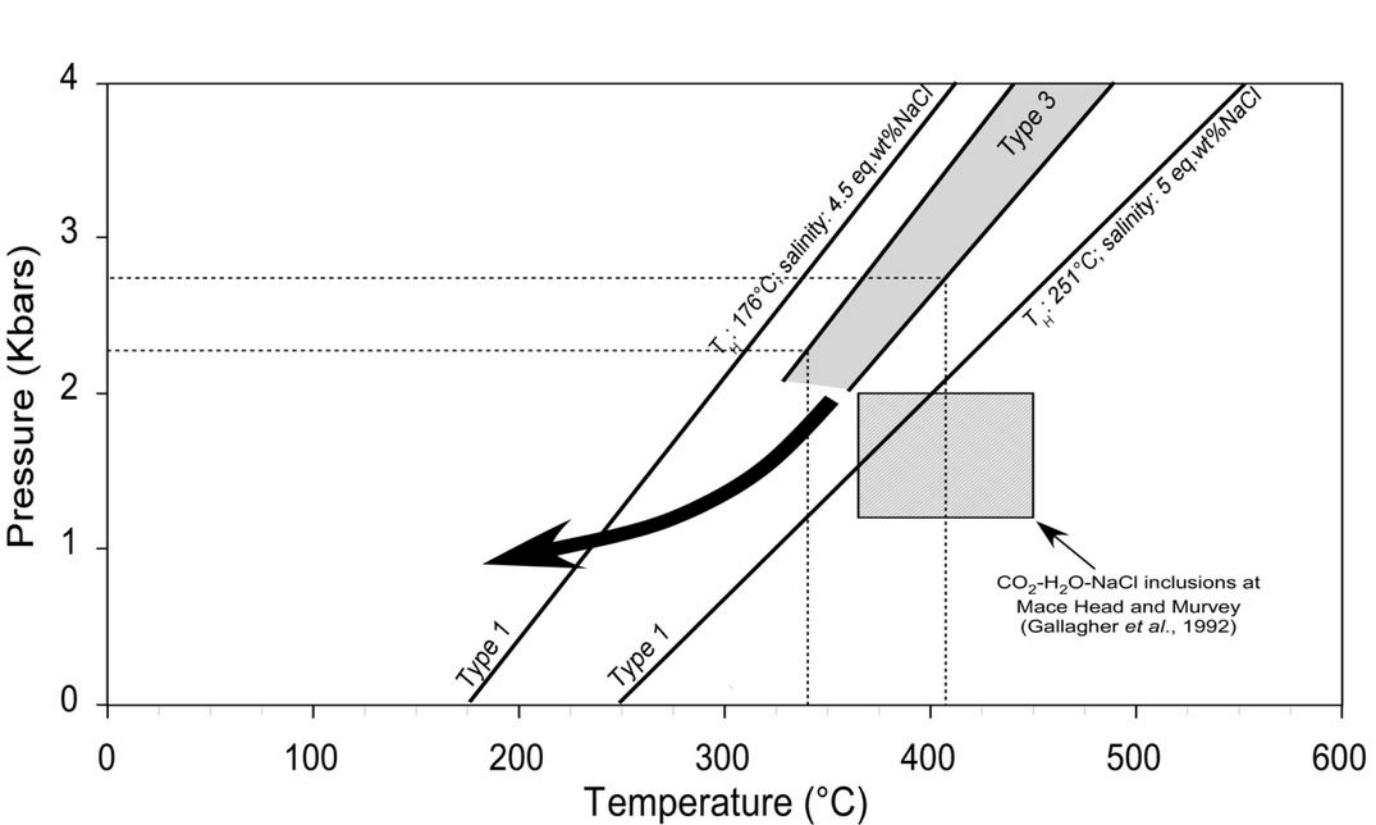
Pressure (Kbars)
Temperature (°C)
0
1
2
3
4
0
100
200
300
400
500
600
Type 3
Type 1
Type 1
T_H: 176°C; salinity: 4.5 eq.wt%NaCl
T_H: 251°C; salinity: 5 eq.wt%NaCl
CO_2-H_2O-NaCl inclusions at
Mace Head and Murvey
(Gallagher *et al.*, 1992)

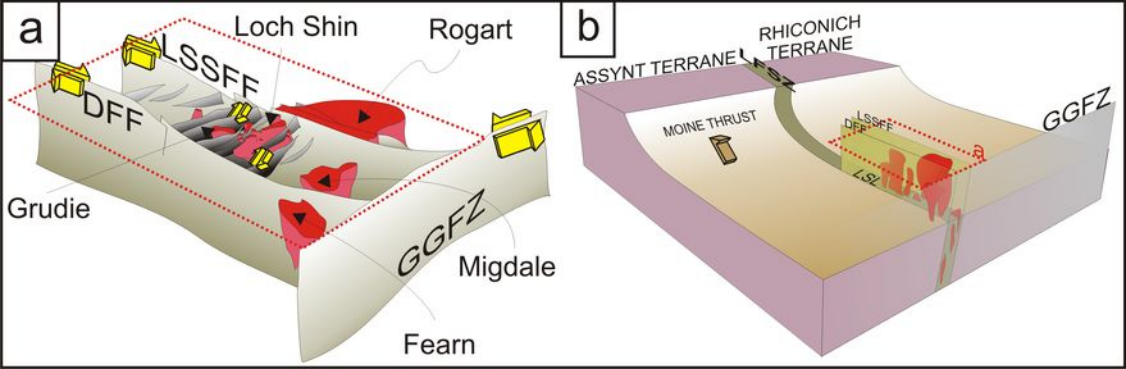
a
Loch Shin
Rogart
LSSFF
DFF
Grudie
GGFZ
Migdale
Fearn
b
RHICONICH
TERRANE
ASSYNT TERRANE
LSZ
MOINE THRUST
LSSFF
DFF
GGFZ
LSZ

School of Earth and Environmental Sciences, University of Portsmouth								Data for Tera-Wasserburg plot2					Data for Wetherill plot2						Ages2							
Identifier	Comments	Beam (um)	U (ppm)1	Th (ppm)1	Th/U	$^{206}Pb/^{204}Pb$	1s%	$^{238}U/^{206}Pb$	1s	$^{207}Pb/^{206}Pb$	1s		$^{207}Pb/^{235}U$	1s	$^{206}Pb/^{238}U$	1s	Rho	$^{207}Pb/^{206}Pb$	1s abs	$^{206}Pb/^{238}U$	1s abs	$^{207}Pb/^{235}U$	1s abs	% conc5	
Sample DS1-11																										
DE10A05		25x37	254	112	0.44	3925	37	3.494	0.039	0.106	0.001		4.188	0.061	0.286	0.003	0.8	1725	16	1622	18	1672	25	94	
DE10A06		25x37	208	92	0.44	2414	32	3.251	0.038	0.107	0.001		4.716	0.070	0.308	0.004	0.8	1742	16	1729	20	1770	26	99	
DE10A07		25x37	241	267	1.11	971	22	14.451	0.172	0.055	0.001		0.536	0.012	0.069	0.001	0.5	431	8	431	5	436	10	100	
DE10A08		25x37	335	384	1.15	1722	37	14.558	0.258	0.056	0.001		0.523	0.012	0.069	0.001	0.6	435	8	428	8	427	10	99	
DE10A09		25x37	105	61	0.58	2739	37	3.222	0.041	0.108	0.001		4.775	0.093	0.310	0.004	0.9	1771	18	1743	22	1780	35	98	
DE10A11		25x37	465	481	1.03	505	40	14.738	0.235	0.056	0.001		0.541	0.011	0.068	0.001	0.5	444	8	423	7	439	9	95	
DE10A12		25x37	266	228	0.85	891	30	14.558	0.166	0.055	0.001		0.521	0.010	0.069	0.001	0.6	427	6	428	5	426	8	100	
DE10A13	High 204Pb - rejected	25x37	105	161	1.54	316	32	14.490	0.197	0.071	0.002		0.695	0.023	0.069	0.001	0.8	945	22	430	6	536	18	46	
DE10A14		25x37	51	30	0.59	790	30	4.452	0.070	0.084	0.001		2.662	0.065	0.225	0.004	0.8	1285	19	1306	21	1318	32	102	
DE10A15		25x37	141	154	1.1	348	27	15.079	0.188	0.056	0.001		0.506	0.012	0.066	0.001	0.6	454	9	414	5	416	10	91	
DE10A16		25x37	282	259	0.92	1135	27	14.817	0.332	0.055	0.001		0.527	0.019	0.067	0.002	0.8	432	9	421	9	430	15	97	
DE10B05		15x27	220	412	1.87	1814	30	14.974	0.322	0.056	0.002		0.522	0.013	0.067	0.001	0.2	446	13	417	9	426	11	93	
DE10B06	High 204Pb - rejected	15x27	538	690	1.28	566	34	14.391	0.238	0.080	0.002		0.769	0.020	0.069	0.001	0.3	1209	32	433	7	579	15	36	
DE10B07		15x27	253	209	0.83	1225	28	13.377	0.211	0.059	0.001		0.634	0.012	0.075	0.001	0.6	572	9	465	7	499	10	81	
DE10B08		15x27	64	77	1.19	399	30	14.353	0.260	0.055	0.002		0.518	0.022	0.070	0.001	0.5	429	16	434	8	424	18	101	
DE10B09		15x27	123	187	1.52	615	49	14.502	0.214	0.055	0.001		0.521	0.015	0.069	0.001	0.6	409	10	430	6	426	13	105	
DE10B10		15x27	144	191	1.33	583	33	14.305	0.193	0.056	0.001		0.539	0.012	0.070	0.001	0.5	436	9	436	6	438	10	100	
DE10B11		15x27	290	403	1.39	1043	27	13.439	0.219	0.061	0.001		0.628	0.014	0.074	0.001	0.5	638	13	463	8	495	11	73	
DE10B12	High 204Pb - rejected	15x27	674	1044	1.55	242	31	16.761	0.403	0.124	0.008		0.930	0.041	0.060	0.001	-0.9	2021	134	374	9	667	30	18	
Standard GJ-1																										
DE10AA04		30x45	389	26	0.04	1301	26	10.158	0.095	0.060	0.001		0.807	0.011	0.098	0.001	0.3	594	8	605	6	601	9	102	
DE10AA12		30x45	266	11	0.04	1245	28	10.125	0.091	0.060	0.001		0.821	0.014	0.099	0.001	0.4	605	9	607	5	609	11	100	
DE10AA17		30x45	310	9	0	1178	28	10.127	0.143	0.060	0.001		0.818	0.012	0.099	0.001	0.7	609	7	607	9	607	9	100	
DE10A04		30x45	300	13	0.04	1306	27	10.133	0.086	0.060	0.001		0.828	0.011	0.099	0.001	0.6	602	6	607	5	613	8	101	
DE10A10		30x45	292	13	0.04	1205	27	10.151	0.087	0.060	0.001		0.826	0.011	0.099	0.001	0.7	613	6	606	5	611	8	99	
DE10A17		30x45	289	12	0.04	1441	36	10.161	0.097	0.060	0.001		0.822	0.012	0.098	0.001	0.7	600	7	605	6	609	9	101	
DE10B04		30x45	270	12	0.04	1176	42	10.155	0.118	0.060	0.001		0.831	0.013	0.098	0.001	0.7	590	7	605	7	614	10	103	
DE10B13		30x45	267	11	0.04	965	34	10.179	0.120	0.059	0.001		0.814	0.013	0.098	0.001	0.7	580	7	604	7	605	10	104	
Standard Temora 2																										
DE10AA05		30x45	141	83	0.6	1043	30	15.103	0.234	0.055	0.001		0.509	0.010	0.066	0.001	0.4	429	9	413	6	418	8	96	
DE10AA06		30x45	143	85	0.6	1313	23	14.686	0.180	0.055	0.001		0.518	0.010	0.068	0.001	0.4	415	8	425	5	424	8	102	
DE10AA07		30x45	145	86	0.6	1067	36	14.767	0.181	0.055	0.001		0.514	0.010	0.068	0.001	0.4	426	8	422	5	421	8	99	
DE10AA08		30x45	144	100	0.7	1122	31	14.805	0.189	0.055	0.001		0.511	0.010	0.068	0.001	0.4	427	8	421	5	419	8	99	
DE10C05		30x45	373	205	0.5	845	28	14.813	0.194	0.055	0.001		0.504	0.009	0.068	0.001	0.7	417	6	421	6	415	8	101	
DE10C06		30x45	327	193	0.6	1187	34	14.974	0.206	0.055	0.001		0.498	0.009	0.067	0.001	0.7	411	6	417	6	410	7	101	
De10C14		20x30	346	188	0.5	1042	34	15.231	0.177	0.055	0.001		0.504	0.009	0.066	0.001	0.7	416	6	410	5	414	8	98	
De10C15		20x30	292	163	0.6	1063	29	15.126	0.180	0.055	0.001		0.501	0.009	0.066	0.001	0.6	414	6	413	5	413	7	100	

1 concentration uncertainty c.20%

2 data not corrected for common-Pb

*3 Concordance calculated as (206Pb-238U age/207Pb-206Pb age)*100*

Decay constants of Jaffey et al 1971 used

Table II.

Sample	Location	wt	Re (ppm)	±	^{187}Re (ppm)	±	^{187}Os (ppb)	±	Age (Ma)	±	± (λ^{187}Re uncert)
Loch Shin											
AF33-10	Loch Shin, NC 56139, 06495	0.021	1.67	0.01	1.05	0.01	7.5	0.0	427.9	2.8	3.1
Gruide Granite											
AF36-10	Moly Burn (Gallagher & Smith, 1975), NC 51530, 04646	0.012	3.53	0.03	2.22	0.02	15.9	0.1	429.6	5.2	5.6
AF01-11	Edge of Grudie Granite NC 52726, 03797	0.014	3.40	0.03	2.14	0.02	15.4	0.1	429.9	5.2	5.6
AF02-11	Edge of Grudie Granite NC 52726, 03797	0.010	8.04	0.05	5.05	0.03	36.1	0.2	428.0	3.0	3.3

Fluid Inclusion Types	Loch Shin granite	Gruide granite	
	sample AF33-10	sample AF35-10	sample AF02-11
Type 1 two-phase (L+V) liquid-rich aqueous inclusions 9-25 µm; sub-rounded and irregular shapes; occur in trails aligned within annealed fractures; some clusters [1]fluid composition: H_2O-NaCl±KCl±CO_2	F: 0.85-0.9 T_{FM}: -45.5° to -50.5° (mean: -47.9°C; N=7) T_{LM}: -13.5° to -1.1° (mean: -6.9°C; N=17) Salinity: 1.9 to 17.3 eq. wt%NaCl (mean: 9.7; N=17) T_H→L: 119° to 170.1° (mean: 152.9°C; N=20) Abundant	F: 0.8-0.95 T_{LM}: -3.6° to -0.7° (mean: -2.8°C; N=20) Salinity: 1.2 to 5.9 eq. wt%NaCl (mean: 4.4; N=20) T_H→L: 151° to 244.4° (mean: 185.6°C; N=20) Abundant	F: 0.7-0.9 T_{FM}: -22.5° to -23° (mean: -22.8°C; N=2) T_{LM}: -4.3° to -2.2° (mean: -3.3°C; N=20) Salinity: 3.7 to 6.9 eq. wt%NaCl (mean: 5.4; N=20) T_H→L: 214.2° to 279.5° (mean: 258.3°C; N=20) Abundant
Type 2 monophase (L) liquid aqueous inclusions 1-5 µm; rounded to sub-rounded shapes; occur in trails within annealed fractures and randomly distributed fluid composition: H_2O-NaCl	[2]Trapping T < 50°C Abundant	Trapping T < 50°C Abundant	Trapping T < 50°C Abundant
Type 3 three- phase (L+L+V) aqueous-carbonic inclusions 4-17 µm; elongated and irregular shapes; occur in trails aligned within annealed fractures; isolated or in clusters fluid composition: H_2O-CO_2.NaCl±H_2S±H_2	F: 0.8-0.9 Common	F: 0.8-0.9 T_{MCO2}: -57.1° to -56.5° (mean: -56.7°C; N=20) T_{Mclath}: 7.2° to 8.2° (mean: 8°C; N=18) T_{HCO2}→fading: 30.5° to 31.1° (mean: 30.8°; N=20) Salinity: 3.6 to 5.4 eq. wt%NaCl (mean: 4; N=18) Density: 0.468 g/cm^3 T_{HTOT}→L: 228.2° to 261° (mean: 243.5°C; N=20) Abundant	F: 0.4-0.85 T_{MCO2}: -57.2° to -56.2° (mean: -56.7°C; N=17) T_{Mclath}: 5.6° to 9.9° (mean: 7.2°C; N=19) T_{HCO2}→L: 28° to 30.9°; T_{HCO2}→fading 31.1° Salinity: 0.2 to 8.1 eq. wt%NaCl (mean: 4.4; N=19) Density: 0.468 to 0.655 g/cm^3 T_{HTOT}→L: 262° to 312.5° (mean: 243.5°C; N=10) T_{HTOT}→V: 305° to 348° (mean: 332.7°C; N=3) Abundant
Type 4 monophase (L) carbonic inclusions 5-10 µm; rounded to sub-rounded shapes; occur in trails aligned within annealed fractures; some isolated fluid composition: CO_2±H_2S	Rare	Not Observed	Rare

Classification is based upon FI morphology and the volumetric proportion of phases observed at room temperature. L = liquid, V = vapour. [1]Bulk composition based on combined microthermometry and Raman spectroscopy. [2]The presence of monophase aqueous liquid FIs indicate trapping temperatures of < 50°C. ± : trace or minor constituent. T_{FM}: temperature of first ice melting; T_{LM}: temperature of last ice melting; T_{HTOT}→L: homogenisation temperature (to L); T_{HTOT} →\ homogenisation temperature (to V); T_{Mclath}: temperature of clathrate melting; F: degree of fill; F=vol. liquid / (vol. liquid+vol. vapour).

Appendices for Holdsworth et al. *Silurian-Devonian magmatism, mineralization, regional exhumation and brittle strike-slip deformation along the Loch Shin Line, NW Scotland*

Appendix A

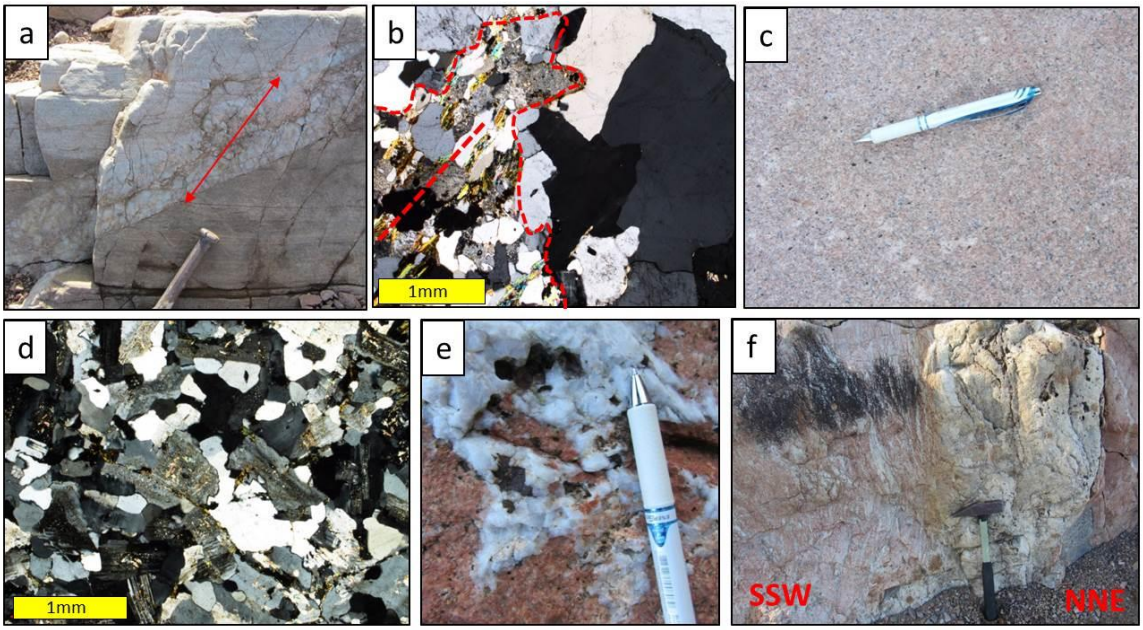

The country rocks, Loch Shin granite and associated veins viewed in the field and thin section. **a)** Oblique view looking down onto undeformed granite pegmatite vein (077/55 NNW) cutting ACW of compositional banding in Moine psammites (100 metres to the SE of the Loch Shin granite (NC 5639 0613). Arrow shows inferred direction of vein opening based on offsets of thin semipelite layer. **b)** Thin section of undeformed granite pegmatite vein shown in (a) cross-cutting S0-S1-S2 fabric in Moine psammites (dashed yellow line). View in crossed polars, with igneous contact shown in red. **c)** Plan view in the field (NC 5631 0650) and **d)** in thin section (crossed polars) of typical undeformed Loch Shin granite (NC 5635 0631). **e)** Close-up plan view of irregular quartz-pyrite veins cutting Loch Shin granite (NC 5631 0650). **f)** Cross-section view of large NW-SE-trending quartz-galena veins (107/85N) cutting Loch Shin granite (NC 5630 0659).

Appendix B

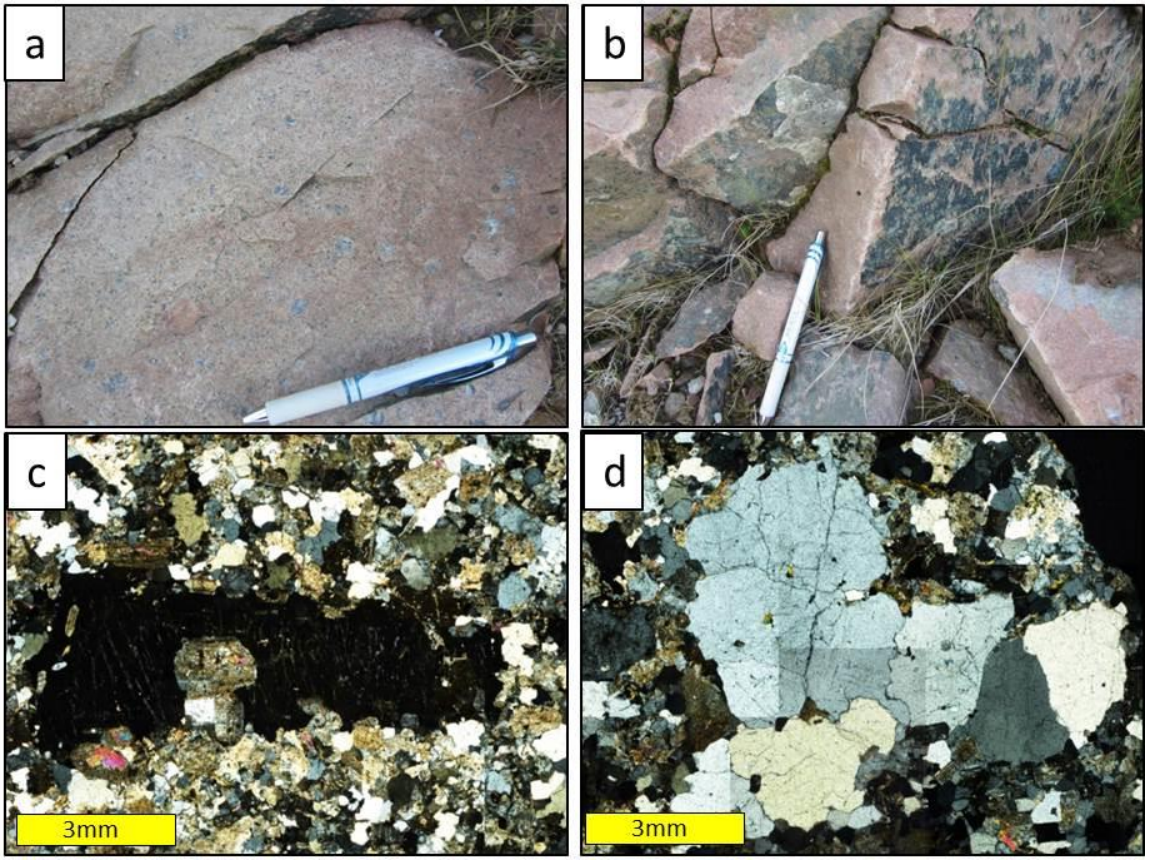

Field and thin section views of the Grudie granite. **a)** Plan view of typical unfoliated Grudie granite with large pink K-feldspar and grey quartz phenocrysts/xenocrysts (NC 5268 0450). **b)** Oblique section view of slickenlined joints with chlorite and epidote mineralization (NC 5267 0444). **c)** Thin section of typical K-feldspar (in extinction) and **d)** polycrystalline quartz xenocryst/phenocrysts within Grudie granite (NC 5310 0427).

Appendix C

ZIRCON U-Pb ISOTOPE ANALYSIS

Sample, mineral separation and analytical protocols

A representative sample of Loch Shin granite from the SW west shore of Loch Shin (DS1-11; Fig. 2b, NC 5635 0625) was selected for Zircon U-Pb LA-ICP-MS geochronology. Zircons were separated from sample DS1-11 using heavy liquids and an isodynamic magnetic separator. The zircon fraction for analysis was handpicked under a binocular microscope and mounted in epoxy resin along with grains of the zircon reference material Temora 2 (Black *et al.* 2004). After polishing and carbon coating, cathodoluminescence (CL) images of the zircons were taken with a KeDev Centaurus CL detector housed on a JEOL 6060LV SEM at the University of Portsmouth (accelerating voltage = 15 kV).

Laser ablation (LA)-ICP-MS U-Pb isotope analyses were undertaken at the University of Portsmouth, using a New Wave 213 nm Nd:YAG laser coupled with an Agilent 7500cs quadrupole ICP-MS. Analytical protocols and instrument conditions are described in detail by Darling *et al.* (2012). Key points of the methodology are: (i) line-raster ablation (aspect ratio 1:1.5), in order to minimise time-dependent elemental fractionation; and (ii) external normalisation to the zircon standard Plesovice (Slama *et al.* 2008) using a 30 μm beam diameter. Laser beam diameters used on unknown zircons ranged from 30 to 15 μm, reflecting the scale of target domains within the crystals. Accuracy was monitored via analyses of the zircon reference materials Temora 2 and GJ-1. Eight analyses of Temora 2 (20 to 30 μm beam diameter) yield a U-Pb concordia age of 417.4 ± 3.5 Ma, and eight analyses of GJ-1 (30 μm beam diameter) yield a U-Pb concordia age of 606.6 ± 3.8 Ma: both of which are within uncertainty of the ID-TIMS reference ages for these materials (Black *et al.* 2004, Jackson *et al.* 2004).

Appendix D

RHENIUM-OSMIUM MOLYBDENITE GEOCHRONOLOGY

Mineral separation and analytical protocols

Molybdenite samples present in the area of the Grudie Granite were isolated using traditional methods of crushing, heavy liquids, and water flotation (Selby & Creaser, 2004). In contrast, given the minor abundance of molybdenite in the Loch Shin Granite sample (AF33-10), and to avoid losing molybdenite during crushing, the mineral separate was achieved using a room temperature HF dissolution of quartz protocol (Lawley & Selby, 2012).

The Re-Os analysis follows that outlined by Selby & Creaser (2004), which determines the Re and Os abundance of the molybdenite using isotope dilution negative thermal ionization mass spectrometry (ID-NTIMS). An aliquant of molybdenite, together with a known amount tracer solution (isotopically normal Os + ^{185}Re) are digested and equilibrated in a carius tube with 1ml 11N HCl and 3ml 15N HNO_3 for 24hrs at 220˚C. Osmium is isolated and purified from the acidic solution using solvent extraction ($CHCl_3$) and micro-distillation methods. The Re is separated and purified using anion chromatography. The separated Re and Os were loaded on Ni and Pt wire filaments with $BaNO_3$ and BaOH activators, respectively, and analyzed for their isotope compositions using NTIMS via static Faraday collection. Analytical uncertainties are propagated and incorporate uncertainties related to Re and Os mass spectrometer measurements, blank abundances and isotopic compositions, spike calibrations, and reproducibility of standard Re and Os isotope values. The molybdenite analyses of this study were conducted during the same period as those of Lawley & Selby (2012). This study reported Re and Os blanks of <4 and 1 pg, respectively, with the ^{187}Os/^{188}Os of the blank being 0.25 ± 0.02 (n = 2). Further, Re-Os model ages determined using the ^{187}Re decay constant of 1.666×10^{-11} a^{-1} (Smoliar *et al.*, 1996) of molybdenite reference materials (NISTRM8599 = 27.6 ± 0.1 and 27.6 ± 0.1 Ma; HLP-5 = 220.0 ± 0.9 Ma), which are in good agreement with their accepted values determined at other laboratories and those previously reported at Durham University (Markey *et al.*, 1998, 2007; Porter & Selby, 2010).

Appendix E

FLUID INCLUSION ANALYSIS

Analytical protocols

Microthermometric analysis was performed on doubly polished wafers (~100 mm thick) using a Linkam THMGS 600 heating freezing stage, mounted on an Olympus transmitted polarised light microscope. The instrument is equipped with a range of special long working distance objective lenses ranging up to 100x magnification. Calibration of the stage was performed using synthetic fluid inclusion standards (pure CO_2 and H_2O). Precision is ± 0.5°C at 300°C and ± 0.2°C at -56.6°C. Following procedures outlined by Shepherd *et al.* (1985), the temperature of first ice melting T_{FM}, the temperature of last ice melting T_{LM} and the temperature of homogenisation T_H were measured in quartz hosted two-phase liquid+vapour inclusions in all wafers (Fig. 9a). Fluid salinities were calculated using T_{LM} and the equations of Bodnar (1993). In addition, clathrate melting temperatures recorded in three-phase (L_{H2O}+L_{CO2}+V_{CO2}) aqueous-carbonic inclusions were used with the equations of Duan *et al.*, (1996) to calculate their fluid salinities (Fig.9b).

Laser Raman Microspectroscopy (LRM) of fluid inclusions was performed using a Horiba LabRam II laser Raman spectrometer. The instrument is equipped with a 600 groove mm^{-1} diffraction grating, a confocal and optical filter system, a Peltier-cooled CCD detector (255 x 1024 pixel array), and is coupled to an Olympus BX51 microscope. Fluid inclusion gas and liquid phases were analysed at room temperature using a 532 nm laser focused through either a 50x or 100x microscope objectives. The spatial resolution of the 532 nm laser at the sample was approximately 2 μm. Individual analyses were performed for between 10 to 60 seconds over the spectral range 1100 cm^{-1} to 4200 cm^{-1}. The number of spectral accumulations per analysis typically ranged between 2 to 5 in order to maximize the signal-to-noise efficiency of the spectrometer. Calibration of the instrument was routinely performed between analyses using the Raman peak of a pure silicon standard (520.7 cm^{-1}). Spectral uncertainty associated with the generation of Raman peak positions is estimated to be ± 1.5 cm^{-1} (2σ; 0.3%) based on replicate analyses of the standard.

Appendix F

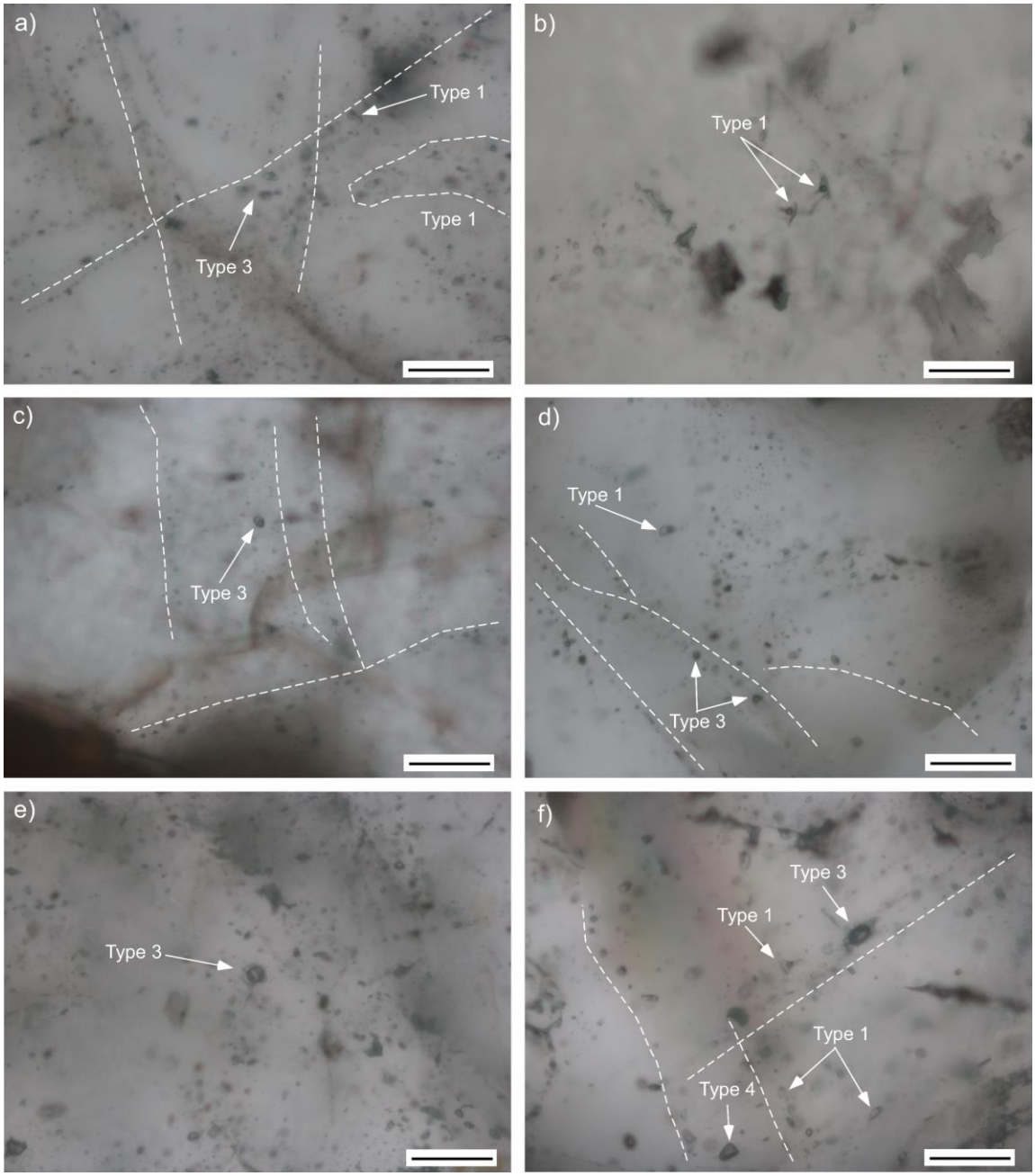

Photographs of fluid inclusions (FI) trails from samples AF33-10 – Loch Shin Granite (**a,b**); AF35-10 (**c,d**) and AF02-10 (**e,f**) both from Gruide Granite. Scale bar = 50 μm.

Appendix G

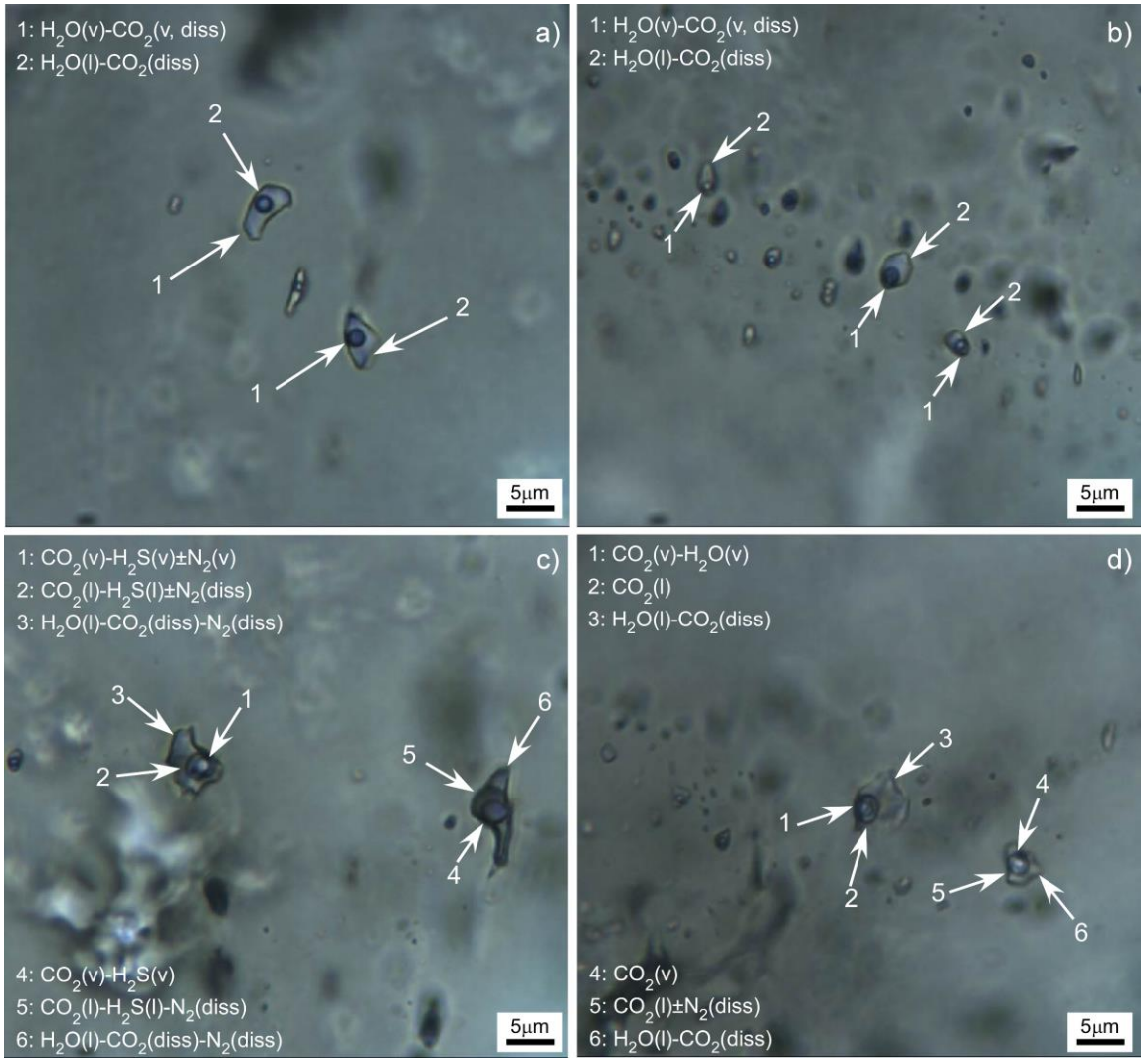

Photomicrographs of Type 1 and Type 3 inclusions within quartz grains in sample AF35-10 (Gruide granite) analysed under Laser Raman Spectroscopy. Type 1 two-phase liquid-rich aqueous inclusions distributed in isolated cluster **(a)** and trails **(b)**. Type 3 three-phase aqueous-carbonic inclusions distributed in clusters (**c** and **d**).

Appendix H:
Re-Os data for molybdenite from Lagalochan Porphyry Cu-Mo system

Sample	location	wt (g)	Re(ppm)	±	187Re(ppm)	±	187Os(ppb)	±	Age	±
RO562-4_RC843047	Hole LD13-1A: 77.45-77.55m depth: 56deg 15' 19.0" N and 05deg 25' 41.1"	0.012	1215.9	5.5	764.2	3.5	5405.0	22.1	423.0	1.7
RO562-5_RC843048	Hole LD13-1A: 115.80-115.90m depth: 56deg 15' 19.0" N and 05deg 25' 41.1"	0.011	254.4	1.2	159.9	0.8	1131.5	4.9	423.2	1.7

Appendix I: Coire Buidhe Fluid Inclusions

Three types of fluid inclusion (Type 1, 2 and 3) were identified in vein quartz from Coire Buidhe (CB1A, B; see Porter & Selby 2010 for sample details), based on their morphology, composition and phase relations at room temperature. Type 1 inclusions are three-phase (liquid H_2O + liquid CO_2 + CO_2 vapour) at room temperature (~25°C). They are found as isolated inclusions, randomly distributed throughout the quartz, and appear to be primary or pseudosecondary in origin. On cooling, the carbonic phase in Type 1 inclusions freezes at ~ -120°C. Melting of the carbonic phase in all inclusions occurs between -57.1 and -56.5°C. Most melting temperatures are close to the triple point of CO_2 (-56.6°C), indicating that the inclusions contain almost pure CO_2. This is confirmed by Laser raman analysis that shows the volatile phase contains < 97.7% CO_2, with minor CH_4, N_2 and H_2S. Clathrate melting, in the presence of liquid CO_2 occurred between 3.7 and 6°C and yields salinities between 7.1 and 11.1 eq. wt% NaCl using the equation of Duan *et al.* (1995) and the software program CLATHRATES (Bakker, 1997). Homogenisation of CO_2 (to the liquid phase) occurs between 27 and 30.4°C, indicating a CO_2 phase density of 0.57 to 0.68 g/cc. Total homogenization to the liquid phase occurs between 291 and 353°C. Type 2 aqueous inclusions are two-phase (liquid + vapour) inclusions and occur along healed microfractures that crosscut quartz grain boundaries. The temperature of first ice melting (T_{FM}) takes place between -20.7 and -23.8° C, close to the eutectic temperature of the H_2O-NaCl-KCl system (-22.9°C). T_{LM} values are between -3.1 and -5.1°C. Clathrate melting between 1.2 and 2.9°C was observed in some Type 2 inclusions. This indicates the presence of non-aqueous phases in Type 2 inclusions. Laser raman analysis of Type 2 inclusions confirmed that the vapour phase contains > 98% CO_2 with minor amounts of CH_4, N_2 and H_2S. Clathrate melting temperatures have been used to calculate salinities of 5 to 5.2 eq. wt% NaCl using software program CLATHRATES (Bakker, 1997). Type 2 inclusions homogenised to the liquid phase (L + V → L) between 261.9°C and 282.9°C.

Type 3 inclusions are found in trails along annealed microfractures, that are occasionally crosscut trails of Type 2 inclusions. First ice melting temperatures were recorded between -21.3 and -24.6°C. T_{LM} values lie between -2.7 and -4.9°C and

correspond to salinities of 4.5 to 7.7 eq. wt% NaCl (Bodnar, 1993). Type 3 inclusions homogenized to the liquid phase (L + V → L) between 165.5 and 218°C.

Additional References Cited in Appendices

Bakker, R.J., 1997. Clathrates: computer programs to calculate fluid inclusion V-X properties using clathrate melting temperatures. *Computers & Geosciences*, **23**, 1-18.

Black, L.P., Kamo, S.L., *et al.* 2004. Improved 206Pb/238U microprobe geochronology by the monitoring of a trace-element-related matrix effect; SHRIMP, ID–TIMS, ELA–ICP–MS and oxygen isotope documentation for a series of zircon standards. *Chemical Geology*, **205**, 115–140, doi: 10.1016/j.chemgeo.2004.01.003.

Bodnar, R.J., 1993. Revised equation and table for determining the freezing point depression of H_2O–NaCl solutions. *Geochimica Cosmochimica Acta*, **57**, 683–684.

Duan Z.H., Møller N., Weare J.H. 1995. Equation of state for the NaCl-H2O-CO2 system: prediction of phase equilibria and volumetric properties. *Geochim Cosmochim Acta,* **59,** 2869–2882

Duan, Z., Moller, N. & Weare, J.H., 1996. A general equation of state for supercritical fluid mixtures and molecular dynamics simulation of mixture PVTX properties. *Geochimica Cosmochimica Acta*, **60**, 1209–1216

Jackson, S.E., Pearson, N.J., Griffin, W.L. & Belousova, E.A. 2004. The application of laser ablation-inductively coupled plasma-mass spectrometry to in situ U–Pb zircon geochronology. *Chemical Geology*, **211**, 47–69, doi: 10.1016/j.chemgeo.2004.06.017.

Markey, R., Stein, H., Hannah, J.L., Zimmerman, A., Selby, D., Creaser, R.A., 2007. Standardizing Re-Os geochronology: a new molybdenite Reference Material (Henderson, USA) and the stoichiometry of Os salts. *Chemical Geology*, **244,** 74-87.

Markey, R., Stein, H., Morgan, J., 1998. Highly precise Re–Os dating for molybdenite using alkaline fusion and NTIMS. *Talanta* **45,** 935–946.

Slama, J., Kosler, J., *et al.* 2008. Plesovice zircon - A new natural reference material for U-Pb and Hf isotopic microanalysis. *Chemical Geology*, **249**, 1–35, doi: 10.1016/j.chemgeo.2007.11.005.

Smoliar, M. I., R. J. Walker, *et al.* (1996). "Re-Os isotope constraints on the age of Group IIA, IIIA, IVA, and IVB iron meteorites." *Science,* **271**: 1099-1102.